2022

Salt Marsh Response to Inlet Switch-Induced Increases in Tidal Inundation

Brian Yellen
University of Massachusetts Amherst, byellen@umass.edu

Jonathan Woodruff
University of Massachusetts Amherst, woodruff@umass.edu

Hannah E. Baranes
University of Massachusetts Amherst

Simon E. Engelhart
Durham University

W. Rockwell Geywer
Woods Hole Oceanographic Institution

See next page for additional authors

Recommended Citation

Yellen, Brian; Woodruff, Jonathan; Baranes, Hannah E.; Engelhart, Simon E.; Geywer, W. Rockwell; Randall, Noa; and Griswold, Fracnes R., "Salt Marsh Response to Inlet Switch-Induced Increases in Tidal Inundation" (2022). *Journal of Geophysical Research: Earth Surface*. 34.
https://doi.org/10.1029/2022JF006815

JGR Earth Surface

RESEARCH ARTICLE
10.1029/2022JF006815

Salt Marsh Response to Inlet Switch-Induced Increases in Tidal Inundation

Brian Yellen[1], Jonathan D. Woodruff[1], Hannah E. Baranes[1,2], Simon E. Engelhart[3], W. Rockwell Geyer[4], Noa Randall[5], and Frances R. Griswold[1]

[1]University of Massachusetts Amherst, Amherst, MA, USA, [2]Gulf of Maine Research Institute, Portland, ME, USA, [3]Durham University, Durham, UK, [4]Woods Hole Oceanographic Institution, Falmouth, MA, USA, [5]Smith College, Northampton, MA, USA

Key Points:

- Inlet and barrier dynamics can have first order controls on tidal propagation and impacts to marshes
- Deposition rates three to five times the rate of sea level rise (SLR) allowed for continued marsh resilience
- Minerogenic sediment supply allowed for marsh resilience under rapid rates of effective SLR

Supporting Information:

Supporting Information may be found in the online version of this article.

Correspondence to:

B. Yellen,
byellen@umass.edu

Citation:

Yellen, B., Woodruff, J. D., Baranes, H. E., Engelhart, S. E., Geywer, W. R., Randall, N., & Griswold, F. R. (2023). Salt marsh response to inlet switch-induced increases in tidal inundation. *Journal of Geophysical Research: Earth Surface*, *128*, e2022JF006815. https://doi.org/10.1029/2022JF006815

Received 29 JUN 2022
Accepted 13 DEC 2022

Author Contributions:

Conceptualization: Brian Yellen, Jonathan D. Woodruff, W. Rockwell Geywer
Formal analysis: Brian Yellen, Jonathan D. Woodruff, Hannah E. Baranes, Simon E. Engelhart
Funding acquisition: Jonathan D. Woodruff
Investigation: Jonathan D. Woodruff, Hannah E. Baranes, Simon E. Engelhart, W. Rockwell Geywer, Noa Randall, Frances R. Griswold
Methodology: Brian Yellen, Jonathan D. Woodruff, Hannah E. Baranes
Project Administration: Jonathan D. Woodruff
Resources: Jonathan D. Woodruff
Visualization: Brian Yellen, Simon E. Engelhart
Writing – original draft: Brian Yellen

Abstract There is widespread concern that rapidly rising sea levels may drown salt marshes by exceeding the rate at which these important ecosystems can build elevation. A significant fraction of marshes reside within backbarrier estuaries, yet little attention has been paid to how changes in inlet geometry influences estuarine tides and marshes. In 1898, a coastal storm eroded a new inlet through the barrier beach that fronts the North-South Rivers Estuary in Massachusetts, USA. The new inlet shortened the North River by 5.6 km and lengthened the South River channel by the same amount. Modern measurements of tidal attenuation suggest that channel shortening abruptly increased mean high tide along the North River by at least 30 cm. Foraminifera communities within North River marsh sediments indicated an environmental change from infrequent to frequent inundation at the time of the 1898 switch in inlet location, which supports this hypothesis. Increased mineral sediment deposition after the inlet switch played a dominant role in allowing marshes along the North River channel to adjust to greater inundation. Following the inlet switch, sediment accreted in North River marshes at 2–5 times the rate of sea level rise (SLR). The North River channel widened by an average of 18% relative to pre-1898 conditions to accommodate the increased tidal prism. The role of mineral sediment accretion in making this marsh resilient to an abrupt increase in inundation depth highlights the importance of maintaining adequate sediment supplies in coastal regions as SLR accelerates.

Plain Language Summary Salt marshes form along sheltered coastlines, incorporating mud and dead roots atop a grassy platform at about the elevation of high tide. It is unclear whether marshes will build their platforms fast enough to keep up with expected increases in sea level. In 1898, a coastal storm eroded a new opening in a beach, behind which a salt marsh extends inland along two tidal channels. The new inlet shortened the distance from the open ocean to parts of the salt marsh, causing high tides that flood the salt marsh to increase more than 30 cm. We considered this "natural experiment" in increased tidal flooding to understand how other marshes might survive rapid sea level rise (SLR). Sediment core samples from the marsh showed that higher tides after the inlet switch resulted in lots of mineral sediment deposited on the marsh platform. This shows that mineral sediment is very important to salt marsh survival when sea level is rising fast. Increased tidal flow after the inlet switch eroded and widened channels. Some of that eroded channel bank sediment deposited atop the marsh, but most of the sediment that allowed the marsh to survive rapid SLR came from the ocean.

1. Introduction

Salt marshes aggrade in quasi-equilibrium with sea level rise (SLR) via the accumulation of organic matter and mineral sediment, thereby maintaining marsh platform elevation within the tidal frame (e.g., Allen, 2000; Cahoon et al., 2019). External perturbations, such as an acceleration of relative SLR, can be compensated for by increased sediment delivery to the marsh platform. Increased inundation depth tends to augment sediment delivery as the associated longer flood duration increases time to trap suspended sediment (Day et al., 1999; Reed, 1990; Temmerman et al., 2003). In some cases, increased suspended sediment concentrations associated with land clearance has allowed marshes to recover from rapid SLR (Peck et al., 2020; Watson, 2004). In addition to increased mineral sediment delivery, there is some evidence that bioproductivity of low marsh grasses may increase with moderate increases in inundation, with subsequent vegetation drowning at higher levels of inundation (Morris et al., 2002; Voss et al., 2013). However, many studies have found declining biomass with increased

Writing – review & editing: Brian Yellen, Jonathan D. Woodruff, Hannah E. Baranes, Simon E. Engelhart, W. Rockwell Geywer, Noa Randall, Frances R. Griswold

inundation, especially among high marsh grass species (Kirwan & Guntenspergen, 2015; Payne et al., 2019; Snedden et al., 2015).

Under moderate rates of relative SLR, marshes can persist for thousands of years by building vertically (Pederson et al., 2005; Redfield, 1972) and/or transgressing into uplands (Doyle et al., 2010; Fagherazzi et al., 2019; Rampino & Sanders, 1980). Under projected rates of global SLR much higher than 20th century rates (e.g., Horton et al., 2020), some studies have suggested that marshes will not be able to build elevation in pace with rising water levels (Crosby et al., 2016; Spencer et al., 2016). The early Holocene may serve as an analogue for marsh dynamics during rapidly changing sea level as global SLR rates were 10–15 times higher than rates over the last 6,000 years (Emery et al., 1965; Wolters et al., 2010). Submerged salt marsh peat found far offshore dating to the early Holocene indicates that marshes may fail when SLR exceeds their ability to build elevation or when SLR-driven shoreline transgression removes the protective morphologies (e.g., barrier beaches) that enable marsh development. Many studies have modeled SLR rate thresholds for marsh survival under various projections of future SLR using known relationships between marsh inundation, sediment supply, and observed vegetative response to changing inundation depth (D'Alpaos et al., 2007; French, 2006; Kirwan & Guntenspergen, 2010; Langston et al., 2020). In general, models suggest that marshes can survive high rates of SLR, but these model results are in disagreement with observations of comparatively lower maximum marsh accretion rates (Coleman et al., 2022). While models are useful for their explanatory power and low cost relative to observational studies, they are simplifications of complex processes with associated limitations (Fagherazzi et al., 2012). Physical experiments likewise have limitations, as testing the effect of rapidly rising sea level on whole tidal marsh resilience would be impractical, prohibitively expensive, and require decades of observations.

While it is impossible to directly observe how salt marshes will respond to sustained accelerated SLR in the future, we can make use of past instances of rapid increases in tidal inundation to inform our understanding of factors that improve marsh resilience to rapid SLR. Several examples exist of changes in tidal dynamics or land elevation leading to rapid, local increases in tidal inundation and impacts to marshes. Removal of tidal restrictions such as undersized culverts can in some cases increase the height of high tide and the resulting tidal inundation of the marsh platform. Boumans et al. (2002) showed that removal of tidal restrictions should be done with care, as the rapid increase in inundation could further stress degraded marshes, especially those that subsided while tides were restricted. However, in some cases these restrictive barriers have served as the catalyst for tidal wetland formation by decreasing hydrodynamic energy, thereby increasing sediment trapping and aggradation leading to wetland creation (McKeon et al., 2022; Meier, 2004; Yellen et al., 2021). Inlet dredging can increase tidal prisms (defined as the volume of water that enters an estuary during flood tide) within sheltered estuaries, causing shifts in marsh regime from largely depositional to erosional (Chant et al., 2021; Van Dyke & Wasson, 2005). Subsidence due to groundwater and hydrocarbon withdrawal can also cause locally accelerated relative SLR (Kolker et al., 2011), and when paired with reductions in terrigenous sediment delivery, has led to tidal wetland loss due to internal ponding (Morton et al., 2005; White & Tremblay, 1995). Conversely, Watson (2004) showed that a California salt marsh actually was able to withstand ∼1 m of subsidence in the 20th century due to increased sediment delivery from the watershed associated with land clearance.

Tectonic events that result in coastal subsidence can quickly increase sea level relative to tidal marsh elevation. At many estuaries adjacent to the Cascadia Subduction Zone (northern California, Oregon, and Washington USA; British Columbia, Canada), sediment records provide evidence for repeated transitions of salt marsh to intertidal mudflat following earthquakes that increased relative sea level in excess of 0.5 m (Atwater & Hemphill-Haley, 1996). Subsequent reestablishment of the marsh is recorded in the sedimentary record as couplets, with mineral rich sediment overlying organic-rich soils or peats that grade back into organic salt marsh sediments (Shennan et al., 1996). Rapid, seismically-induced subsidence along active margins is typically followed by uplift that reduces the rate of relative SLR once the tectonic plates become coupled again (Peck et al., 2020). While the role of tectonics in driving changes to relative sea level and marsh response has been well documented, marsh impacts from changing barrier/inlet dynamics and resultant tidal adjustments are less certain.

On passive margins, where salt marshes are more common, barrier/inlet dynamics often mediate tidal propagation and salt marsh development (FitzGerald et al., 2020; Hein et al., 2012; O'Brien, 1969). Landward of barrier island complexes, Lucke (1934) highlighted the tendency for tidal marshes to initiate on flood-tide deltas, with differing marsh morphologies forming behind stable versus migrating inlets. Migration of inlet locations can affect tidal marsh sedimentation rates too; marine sediment is often delivered to marshes through inlets, so

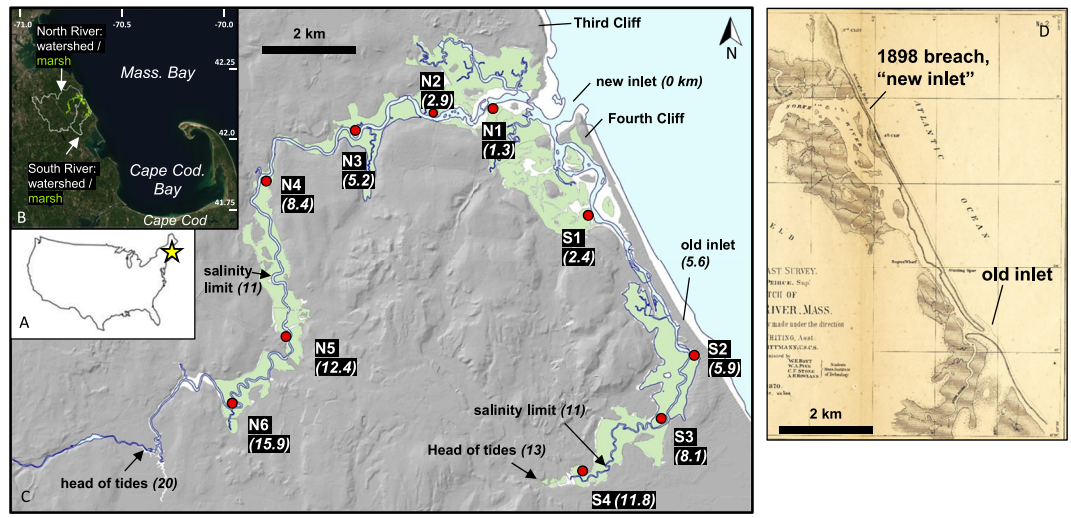

Figure 1. Site map of the North-South Rivers Estuary. Red dots correspond to core transect and water level observation locations; numbers in parentheses refer to river distance to the inlet in km. Marsh area (National Wetlands Inventory, 2013) is depicted with green, intertidal mudflat and beach in white, and upland is shaded in gray. Panel (d) at right shows the North South Rivers Estuary barrier beach as depicted in an 1870 chart (Peirce et al., 1870).

increased proximity to the inlet drives enhanced delivery of mineral sediment and increased sedimentation rates (Roman et al., 1997). The spacing between tidal inlets is controlled in large part by tidal range, with larger tidal prisms requiring more closely spaced inlets (FitzGerald, 1988; Hayes, 1979), which in turn can control the size and distribution of individual marshes within lagoons (Friedrichs & Perry, 2001). However, the impact of abrupt inlet location changes on backbarrier marshes is relatively understudied, despite the relatively frequent nature of barrier breaching and new inlet formation driven by storms (e.g., Buynevich & Donnelly, 2006; FitzGerald & Pendleton, 2002; Hayes & FitzGerald, 2013; Italiani et al., 2020).

Here we make use of an historic barrier breach and change in tidal inlet location to the North-South Rivers Estuary, first to illustrate how the estuary's tidal marsh responded to resultant increased tidal elevations, and second to show the role of inlet location in controlling tidal propagation up estuarine channels. To our knowledge, this is the first study to highlight the first order control of inlet location on tidal heights and salt marsh response. Results from this study can help guide tidal marsh restoration involving the removal of tidal restrictions, which can also result in a step increase in salt marsh inundation depths and encourage coastal management practices that treat sediment as a valued resource.

2. Site Description

2.1. North-South Rivers Estuary

The North-South Rivers comprise a bar-built estuary, whose channels connect to the mesotidal Massachusetts Bay via a shared inlet (Figure 1). At its inlet, the North-South Rivers Estuary's tidal range is about 3.5 m (Buynevich & Donnelly, 2006), with that range decreasing up-estuary (Baranes et al., 2022). Channel widths of the North and South Rivers are approximately 100 m within their seaward reaches, and narrow landward. The tidal reach for the larger North River is 20 km compared to 13 km for the South River. Both tidal channels are fringed by a high marsh platform that is generally 300–500 m in width and dominated by *Spartina patens* and short form *Spartina alterniflora*. Limited low marsh areas are confined to channel proximal areas less than 2 km from the present inlet, where the estuary has more of an open embayment morphology rather than a confined channel. Limited dredging has been done at the estuary inlet and along the South River channel within 3 km of the inlet, though efforts have been hindered by the cobble river bottom that is unsuitable for hydraulic dredging (personal communication, Michael DiMeo, 11 October 2022). The North River channel has not been dredged since at least 2000, as generally high tidal velocities maintain the channel. Previous work investigating the timing of increased turbidity within the North and South Rivers and sediment deposition on the marsh platform showed that marine sediment delivered on the flood tide during coastal storms provides the primary source of suspended

sediment to the estuary and marsh (Baranes et al., 2022). Suspended sediment inputs from the watersheds of the North River (area = 210 km^2) and South River (area = 60 km^2) are relatively minor (Baranes et al., 2022) due to low relief and low sediment yields associated with the region's post-glacial landscape (e.g., Cook et al., 2015; Ralston et al., 2020).

Relative SLR at the Boston tide gauge, 35 km to the north, has averaged 2.87 ± 0.15 mm/yr during 1920–2020 (NOAA gauge 8443970), and 3.6 mm/yr during 1987–2017 (Talke et al., 2018). Salt marsh accumulation rates for the last 100 years average 4.0 mm/yr at sites 40–60 km to the south that have similar tide range, physiography, and species compositions to those observed at North and South Rivers (O'Keefe Suttles et al., 2021).

2.2. The 1898 Portland Gale and Recent History

During the 1600s to the late 1800s, the sole inlet for the North and South Rivers was located at what is now Rexhame Beach in the town of Marshfield, MA (Figure 1, old inlet). In 1898, a strong late November storm cut a new inlet through the barrier beach that previously connected two eroding drumlin headlands known as Third Cliff and Fourth Cliff. These headlands serve as predominant sources of sediment to the Scituate/Marshfield regional beach complex (Woodruff et al., 2021). Subsequently named "The Portland Gale of 1898" after the tragic sinking of the steamship *SS Portland* during the storm, the 1898 Portland Gale remains among the top 10 coastal floods of record in the region (Talke et al., 2018). Firsthand accounts of the storm suggest that fluvial flooding during the storm caused the wave-compromised barrier between Third and Fourth Cliffs to fail. The old, more southerly inlet closed by 1900 (Freitas & Ball, 1995), with the new northern inlet resulting in a 5.6 km shortening of the North River channel and equal lengthening of the South River (Figure 1) (Buynevich & Donnelly, 2006). Accounts of the storm's aftermath noted increased frequency of high marsh flooding along the North River after the inlet switch (Freitas & Ball, 1995).

We make use of this natural experiment of an abrupt change in inlet location and channel shortening to observe resultant impacts to tidal heights and salt marsh inundation along the North and South Rivers. We combine water column observations, elevation surveys, and sediment cores to evaluate what conditions allowed the estuary's marsh to survive this stressor. Observations from these systems can provide useful guidance to coastal managers regarding conditions that may allow marshes to survive increased inundation due to projected near-term SLR acceleration.

3. Methods

3.1. Sediment Cores and Probing

We collected 1 m sediment cores from the marsh platform during 2018 from six channel-perpendicular transects on the North River and four transects along the South River (N1–N6 and S1–S4, see Figure 1 for locations). Roughly 10–15 cores were collected for each transect and described in the field. An additional representative core from each transect was preserved for lab analyses at the University of Massachusetts Amherst. All cores were collected using a 6 cm internal diameter gouge corer, which results in negligible vertical compaction and allows for visual observation in the field (Yellen et al., 2020).

3.2. Sediment Processing

Sediment cores were processed to identify temporal and spatial variability in deposition rates and sediment composition within the North-South Rivers system. Sediment cores were transported to the University of Massachusetts, where they were split, described, and evaluated for down-core elemental abundances via X-ray fluorescence (XRF) core scanning (Croudace et al., 2006). A clear onset of elevated heavy metals evident in the XRF-derived bulk lead profile was used to assess relative sedimentation rates. The bulk lead onset depth is associated with the timing of industrialization, and generally dates to 1850–1900 in this region (Boldt et al., 2010; Bricker-Urso et al., 1989). Lead XRF counts were converted to concentrations according to an empirical regression based on North and South River marsh cores from Baranes et al. (2022).

We subsampled 1 cm-thick sections from sediment cores every 10 cm to assess soil organic matter via loss on ignition (LOI), combusting dried and weighed samples at 550°C for 4 hours (Dean, 1974). In the field and during

core description, we noted a unique stratum present in cores from transects N1, N2, N3, and N4 (see Figure 1 for locations) that was characterized by a reddish-brown color and fibrous, matted texture. We increased sample resolution surrounding this stratum in order to evaluate the lithological changes that characterized the visually observed, widespread change in conditions at the time of deposition. We analyzed two cores, N3C1 and S3C3 in greater detail, subsampling those cores every 5 cm.

We used radiometric dating via down-core ^{137}Cs and ^{210}Pb profiles to constrain the date of the increase in bulk lead (Anisfeld et al., 1999; Cundy & Croudace, 1996). We chose representative cores N3C1 and S3C3 for gamma spectroscopy from transects N3 and S3 based on the following criteria. First, the core had to be a minimum of 20 m from the channel to avoid creek edge impacts that include lateral erosion, levying, and subsidence (Moskalski & Sommerfield, 2012; Roner et al., 2016). Second, the core top elevation was roughly equivalent to median marsh platform elevation (where core top elevations were 0.86 m NAVD88 for N3C1 and 0.98 m NAVD88 for S3C3). Third, the core's XRF-derived bulk lead profile enabled identification of a clear onset and peak in industrial metal contamination.

Approximately ten 1 cm thick subsamples were taken from each core to resolve the onset and peak of ^{137}Cs and the decay of ^{210}Pb. Samples were dried and weighed, then sealed in 70 cm^3 cans to allow for supported ^{210}Pb to be distinguished from unsupported ^{210}Pb. Activities for ^{137}Cs and ^{210}Pb were measured on a Canberra GL2020R Low Energy Germanium Detector for 48–72 hr and computed spectroscopically from the 661.66 keV and the 46.54 keV photopeaks, respectively. Age versus depth models were obtained based on the depletion of ^{210}Pb in core subsamples via the constant initial concentration model (Pennington et al., 1976) and the 1954 CE onset and 1963 CE peak in ^{137}Cs concentrations (Pennington et al., 1973). We assumed that ^{210}Pb-derived ages that indicated age reversals (i.e., a sample with less unsupported ^{210}Pb overlying a sample with greater unsupported ^{210}Pb) were outliers and were not included in linear deposition rate calculations. Radioisotope data are included in Tables S1 and S2 in Supporting Information S1. We used these age models to approximate the timing of the onset of heavy metals contamination in marsh sediments, which can be measured at low cost with XRF core scanning (see above). Past work in the region has shown the initial rise in heavy metals within sediment cores to date to 1850–1900 (Boldt et al., 2010; Bricker-Urso et al., 1989). Baranes et al. (2022) observed lead concentrations as high as 4,000 ppm in marsh cores collected from the North River and linked these extremely high concentrations to activities at a former munitions manufacturing site located directly upstream that began operations in the early 1900s.

3.3. Foraminifera

Foraminiferal assemblages can be used to assess environmental conditions indicative of marsh inundation frequency (Scott & Medioli, 1978). Eight foraminifera samples were processed from core N3C1 according to standard methods (Scott & Medioli, 1980) and summarized here. Core subsamples spanned 1 cm and were obtained roughly every 15 cm, with increased spatial resolution above and below the fibrous stratum noted above in Section 3.2. Samples were washed through sieves to isolate the 63–500 μm fraction and counted wet under a binocular microscope. The greater than 500 μm fraction was checked for larger foraminifera. A minimum of 50 individuals was counted in each sample to ensure that it accurately characterized the assemblage (Kemp et al., 2020). Our taxonomy follows Wright et al. (2011) and references therein. Foraminiferal census data are provided in Table S3 in Supporting Information S1.

3.4. Water Surface Elevation

To assess the elevation of the marsh platform relative to the tidal frame, tidal channel water surface elevation was measured continuously for at least 40 days during March and April of 2018 at N1–N6 and S1–S4 (Figure 1). Pressure transducers were mounted to rebar and deployed in the channel below the lowest low tide level at each location and surveyed to NAVD88 by measuring the water surface elevation over the mooring with a post-processing kinematic GPS every second for 1 min and subtracting the average sensor-measured water depth during the same 1-min interval. Continuous salinity and temperature measurements were collected (RBR model XR-620) adjacent to each pressure transducer and to correct for water density variations. Observations from a subaerial pressure transducer were used to correct water levels for barometric pressure effects. We computed a 1983–2001 National

Tidal Datum Epoch equivalent Mean High Water (MHW) datum at each sensor location using the NOAA Tidal Analysis Datums Calculator with the Boston NOAA gauge as a control station.

3.5. Marsh Surveying and Channel Dimensions

We surveyed marsh platform elevation with real time kinematic (RTK) GPS along each of our 10 channel-perpendicular transects in March of 2018 (red dots in Figure 1). The average horizontal spacing of survey points along transects was 1.5 m. We used a public network of GNSS reference stations (MaCORS) to correct RTK measurements in real time. Horizontal and vertical errors reported by our RTK unit were generally less than 2 cm, consistent with published values for the this method (Aykut et al., 2015).

We compared widths of the main North and South River channels from before and after the 1898 inlet location change to evaluate channel dimension increase/decrease resulting from the inlet switch. To make pre-1898 channel measurements, we georeferenced a detailed 1870 map of the North-South Rivers Estuary (Peirce et al., 1870) that clearly depicted the marsh edge. In a geographic information system, channel widths were measured every 0.25 km along both estuarine channels. To assess changes in channel dimensions, 1870 channel width measurements were compared to similar measurements made along the same transect lines using a 1960 aerial photograph (US Air Force, 1960) and georeferenced to a 2019 orthomosaic aerial photo (MassGIS, 2019). Both the historic map and aerial photo were georeferenced to the 2019 orthomosaic photo using the locations of known landmarks such as road intersections or historic buildings, with 10+ ground control points for each image. We checked the fidelity of georeferenced images by measuring the distances between an independent set of ground control points in the orthomosaic and georeferenced images. Measured distances varied by less than 0.3%, which was an order of magnitude less than the changes in channel width that we intended to detect. Channel width was defined as the distance along open-water channel-perpendicular transects from marsh edge to marsh edge, defined as the line between grass and water. The estuary's channel banks are close to vertical, making this channel width measurement method relatively insensitive to tidal hour at the time of aerial image capture. The dominant source of error with this measurement is the manual interpretation of the exact location of the marsh edge. We made many measurements to overcome this signal noise as has been done in similar studies (e.g., Watson et al., 2017). North River width measurements began 3 km from the new inlet where the estuary transitions from an open embayment morphology to a confined channel, and continue up to the head of tides (river km 20). South River measurements span river km 6.5 to 10, beginning at the old inlet location, and ending at the limit of coverage for the 1870 map.

4. Results

4.1. Deposition Rates, Stratigraphy, and Foraminifera

We used short-lived radionuclides to constrain the deposition rates of representative sediment cores from the North River and South River marshes. The uppermost sample from core N3C1 at 0–3 cm depth exhibited lower unsupported ^{210}Pb activities than the subsequent sample below at 9–10 cm, resulting in an impossibly young modeled date of 2030 for the 9–10 cm sample. We thus treated this uppermost measurement as an outlier, removed it from the age model, and interpolated surface ^{210}Pb activity based on a linear fit with the two underlying samples as has been done for other studies (e.g., Peck et al., 2020; Wheatcroft & Sommerfield, 2005). The deposition rate from this modified N3C1 age model is similar to the deposition rate based on the age model that includes all outlier measurements (Figure S1 in Supporting Information S1). General coherence between ^{210}Pb and ^{137}Cs-derived age constraints adds further confidence to the ^{210}Pb-based age model. The average deposition rate in the upper 72 cm of the North River core (since ~1920) was ~6 mm/yr (Figure 2a). South River deposition during the same period at S3 averaged 3 mm/yr (Figure 2d, Figure S2 in Supporting Information S1). Age models therefore indicate roughly twice as much deposition at N3 than at S3 since ~1900 (Figures 2a and 2d).

During low tide conditions, we observed a visually distinct stratum within the North River channel banks approximately 60–80 cm below the marsh platform that was characterized by erosion-resistance (protruding past other layers) and a reddish color (see photo, Figure S3 in Supporting Information S1). Within marsh gouge cores extending away from the channel, this organic marker horizon was easily visually identified while in the field. Based on rapid field observations of the depth to this layer in cores from the North River, we assessed relative deposition rates away from the channel (Figure S4 in Supporting Information S1). We refer to this layer as the

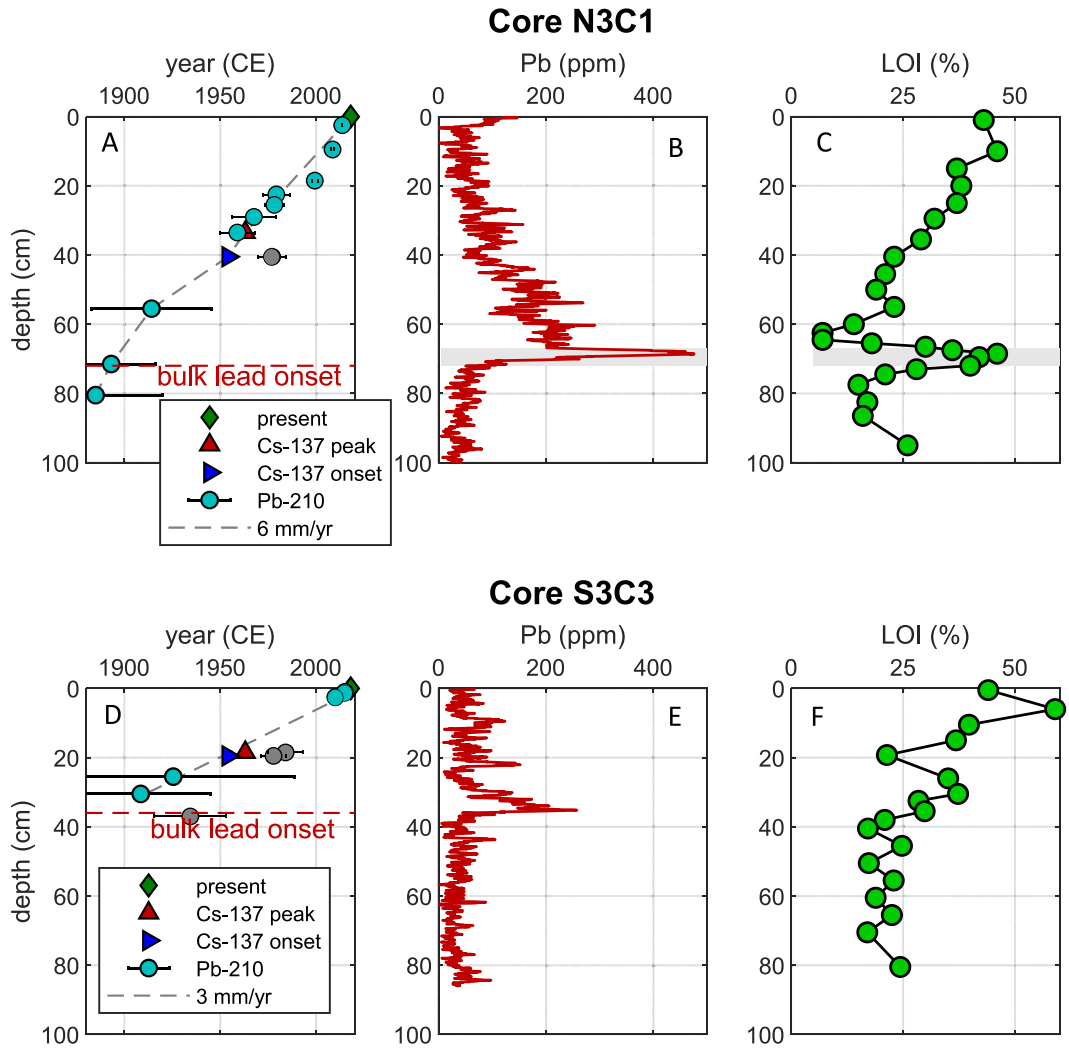

Figure 2. The top row shows observations from our representative N3 transect core (N3C1) and the bottom row shows observations from S3 transect representative core (S3C3). Panels (a) and (d) show age versus depth models for each core, including age controls derived from ^{210}Pb, and ^{137}Cs onset and peak. ^{210}Pb outliers are shown in gray and were excluded from best fit lines. Panels (b) and (e) show Lead profiles from X-ray fluorescence scans in units of ppm based on an empirical regression presented in Baranes et al. (2022). Panels (c) and (f) show loss on ignition profiles versus depth. Gray shaded bars in N3 profiles depict the depth of the visually identifiable marker horizon.

"organic marker horizon" throughout the text. No corresponding layer was observed in South River cores or along South River exposed channel banks.

Bulk lead concentrations and organic content (LOI) profiles from representative N3C1 and S3C3 cores are shown in Figure 2 to relate the date of the heavy metal contamination onset and organic marker horizon to the age model. In core N3C1, the depth of the organic marker horizon described above was clearly depicted by high LOI values between 67 and 70 cm. This organic layer is contemporaneous with a step function rise in bulk lead contamination whose age is consistent with early 1900s opening of an upstream munitions manufacturing plant (Tetra Tech EC, Inc., 2005). LOI values decreased to 7% immediately above the marker horizon indicating an increase in mineral content. This was followed by a gradual increase in organic content and decrease in mineral content toward the surface. In contrast to observations from N3C1, organic content (LOI) in core S3C3 increased above background levels following the increase in bulk lead, whose onset also dated to the turn of the 20th century.

A comparison of the ~1900 onset depth of lead contamination across the estuary indicated higher 20th century accumulation rates along the North River marsh than in the South River marsh, consistent with observations from our two cores dated via gamma spectroscopy (Figure 3). Channel-perpendicular transects showed similar

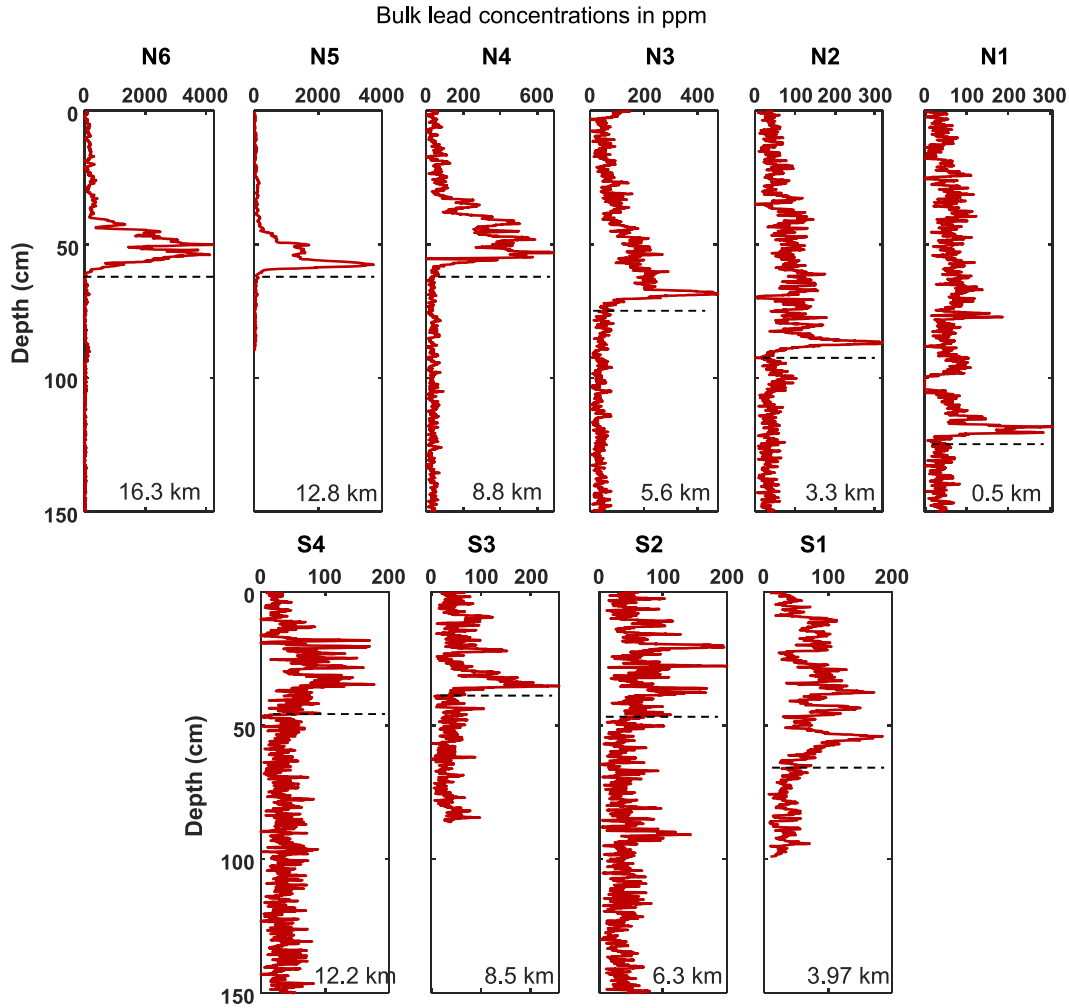

Figure 3. Bulk lead profiles from representative sediment cores from the North River (top row) and South River (bottom row) from ITRAX X-ray fluorescence corescanner data converted to parts per million according to a site-specific empirical regression reported in Baranes et al. (2022) where $PPM_{Pb} = 1.14 * Counts_{xrf} - 0.48$. River distance from the shared NSRE inlet is shown at the bottom of each panel. A dashed black line indicates the onset depth of heavy bulk lead contamination. The *x* axis scale changes between plots to allow for visual resolution of the lead increase. Baranes et al. (2022) explained the up-estuary increase in sediment lead abundance along the North River as evidence of dilution of contaminated watershed sediment by abundant, uncontaminated marine sediment.

amounts of deposition above the organic marker horizon with increasing distance from the channel (Figure S4 in Supporting Information S1). At up-estuary North River transects (N4–N6), the sediment thickness above the lead contamination onset totaled approximately 60 versus 40 cm at S2–S4 in the South River, indicating at least 50% more accumulation in North River marshes since industrialization (Figure 3). At transects N1–N3 and S1, which was between the old and new inlet, lead onset depth increased with proximity to the new inlet, with approximately 122 cm of sediment deposition at site N1 since the initial rise in lead abundance.

Foraminiferal assemblages were enumerated from core N3C1 to assess changes in tidal inundation depth and frequency associated with the organic marker horizon at 67–70 cm depth (Figure 4). The two foraminiferal samples below the organic horizon (70–71 and 75–76 cm) were characterized by an assemblage dominated by *Jadammina macrescens* and *Trochammina inflata* with <1% of low marsh species including *Miliammina fusca*, *Ammobaculites* spp., and *Reophax* spp. We use *Jadammina macrescens* (rather than *Entzia macrescens;* Filipescu & Kaminski, 2011; Schönfeld & Mendes, 2022) because it continues to be widely used in the sea-level literature and this is the taxonomy employed in pre-existing databases of modern assemblages in the region (Kemp et al., 2015 and references therein). At 65–66 cm, below the organic horizon, there was a switch in assemblage

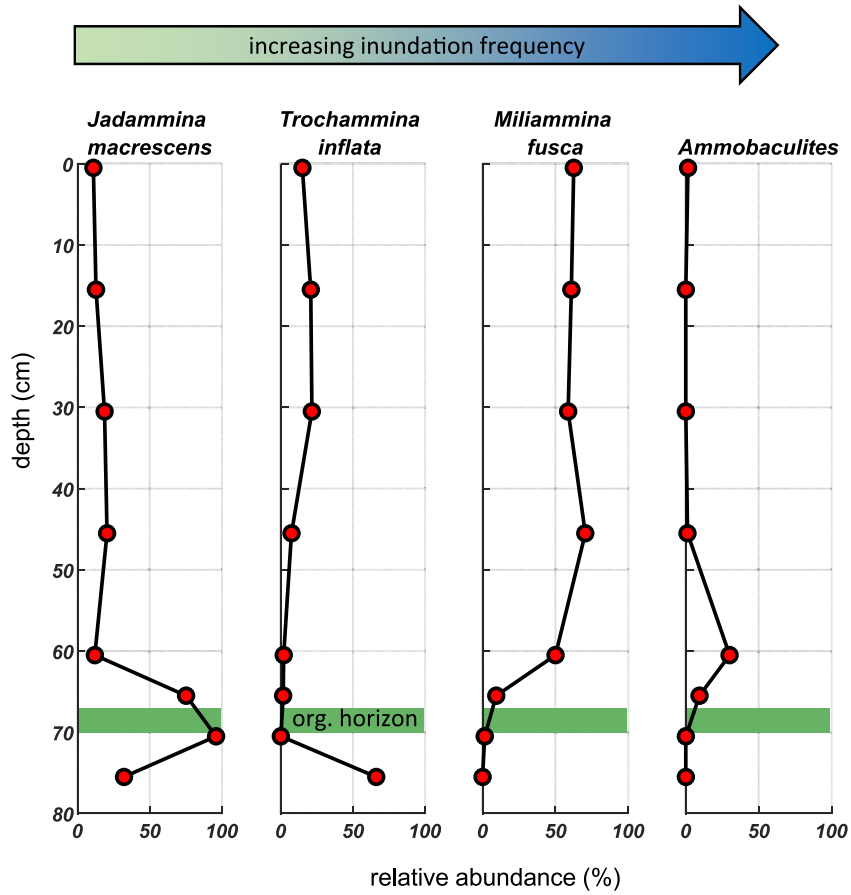

Figure 4. Total abundances of foraminifera taxa by percent in discrete 1 cm sediment samples (see Section 4.1), including *Jadammina macrescens*, *Trochammina inflata*, *Miliammina fusca*, *Ammobaculites*. Taxa are ordered from left to right according to the species elevation optima from Wright et al. (2011) with more frequent inundation on the right. The green shaded interval indicates the depth of the organic marker horizon.

to *M. fusca* (9%), *Ammobaculties* spp. (9%), and *Reophax* spp. (<1%) increased to 19% of the assemblage while continuing to be dominated by J. macrescens (75%). This pattern continues at 60–61 cm with an increase in *M. fusca* (50%) and *Ammobaculites* spp. (30%) to 80% of the assemblage with *J. macrescens* significantly reduced (6%). This trend continues up core at 45–46 cm with increasing *M. fusca* (70%), *J. macrescens* (20%), and *T. inflata* (7%) and a reduction in *Ammobaculites* spp. (1%). Toward the top of the core, there is a reduction in *M. fusca* (61%) and *J. macrescens* (13%) and an increase in *T. inflata* (21%) and *Tiphotrocha comprimata* (5%). Foraminiferal census data are provided in Table S1 in Supporting Information S1.

4.2. Along Channel Tidal Observations

Instrumentally obtained MHW elevations generally decreased with increasing distance from the inlet, with roughly equal tidal attenuation observed in the North and South River channels (dashed lines in Figure 5a). MHW ranged from a maximum 1.50 m NAVD88 near the inlet (location N1) to a minimum of 1.12 m NAVD88 on the South River at S4 (12.2 km from the inlet), and a minimum of 1.11 m NAVD88 on the North River at N5 (12.8 km from the inlet; Figure 5a). On average, MHW elevation decreased 5 cm per km up-estuary from the inlet along both estuarine channels up to 8.5 km from the shared inlet. This trend reversed in the upper reaches of the North River tidal channel, with MHW elevation increasing by 5 cm over the 3.5 km from N5 to N6 (Figure 5b). MHW elevation was approximately 5 cm higher in the North River channel than in the South River at equivalent distances from the inlet within the lower estuary (less than 10 from the mouth) (Figure 5a).

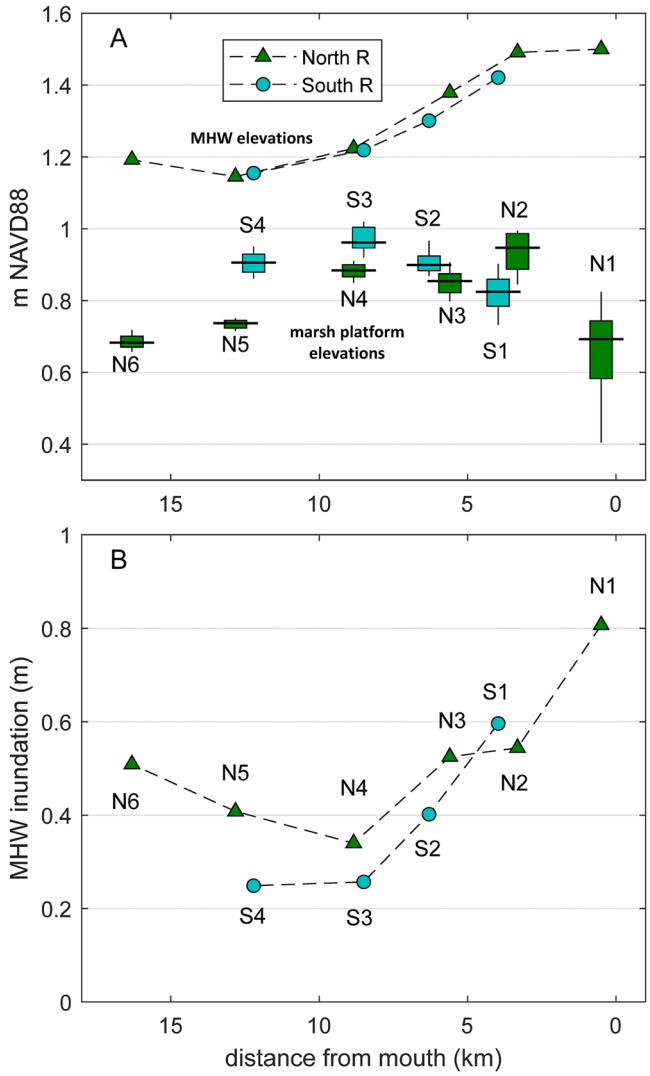

Figure 5. Mean high water (MHW) and marsh platform elevation summary along the North and South Rivers relative to the NAVD88 vertical datum. Panel (a) shows MHW at marsh transect locations (see Figure 1) and summaries of real time kinematic-derived marsh platform elevations at each transect location depicted. Boxes represent the 25th–75th percentiles, and whiskers representing the 10th and 90th percentiles. Panel (b) shows the average marsh inundation depth at each transect calculated as the MHW minus the median marsh platform elevation. Data labels (N1 etc.) correspond to locations depicted in Figure 1. Note that distances from the ocean increase to the left, consistent with our site map.

4.3. Marsh Platform Elevation

Median marsh platform elevation along the North River channel (box plots in Figure 5a) tended to decrease up-estuary, with the exception of low marsh site N1, which is the most exposed to waves from the open inlet and has a dense channel network. Along the South River, median marsh elevation increased up-estuary from sites S1–S3, followed by a decrease from S3 to S4 (Figure 5a). Marsh platform 25th–75th percentile elevations varied less than 10 cm within individual transects at each site (again with the exception of N1). The average 25th–75th percentile elevation range at sites N2, N3, and S1–S4 was 5 cm. At upper estuary sites N4–N6, marsh elevation varied less, averaging 3 cm for the same metric.

We estimated average marsh inundation depth at high tide throughout the estuary by subtracting median marsh elevation from measured MHW values at each transect (i.e., the difference between markers and box plot medians in Figure 5a). Marsh inundation depth at MHW generally decreased up-estuary, ranging from 0.81 m at the mouth (site N1) to 0.25 m at S3 and S4 (Figure 5b). Inundation depths on the South River marsh were less than those on the North River at all equivalent distances from the inlet except S1. Because S1 is located between the old and new inlet locations, the inlet switch did not substantially change its distance from the ocean. High-marsh average inundation depths in the lower estuary (less than 10 km from the inlet) were 0.47 m on the North River (N2–N4) and 0.42 m on the South River (S1–S3). In the upper estuary, (N5, N6, S4), North River marsh inundation averaged 0.46 m, which was nearly double the observed inundation depth of 0.25 m along the upper reaches of the South River (S4).

4.4. Marsh Channel Dimensions

Differences in channel width between the 1870 map, 1960 aerial photo, and 2019 orthomosaic photo indicated a general and continual widening toward the present along the North River (Figure 6). The average total width increase between 1870 and 2019 was 18 ± 3% (mean ± standard error) across the 49 measured locations, with 32 of the locations experiencing >10% widening, and only four experiencing >10% narrowing. There was no spatial trend in this widening (Figure 6b). Of the average 18% widening, a little more than half occurred during 1870–1960, with the remainder of the widening occurring between 1960 and 2019. Based on these observations, channel widening of the North River has been somewhat continual and has averaged about 1.5% per decade.

A similar analysis of channel width adjustment for the South River did not identify any noticeable change in between 1870 and 2019 (Figure 3 in Supporting Information S1). Depiction of the South River on the 1870 map extended upstream only to river km 10.5, and therefore only allowed for 16 width measurements. Of the 16 width change observations, five showed widening and three showed narrowing of more than 10%, with an average widening of 4 ± 3% (mean ± standard error).

5. Discussion

5.1. Marsh Accumulation Rates and Stratigraphy

Based on the timing and stratigraphy surrounding the organic-rich marker horizon with high lead concentrations evident at transects N1–N4, we interpret the layer as a pre-1898 stable high marsh platform. Prior to the inlet switch,

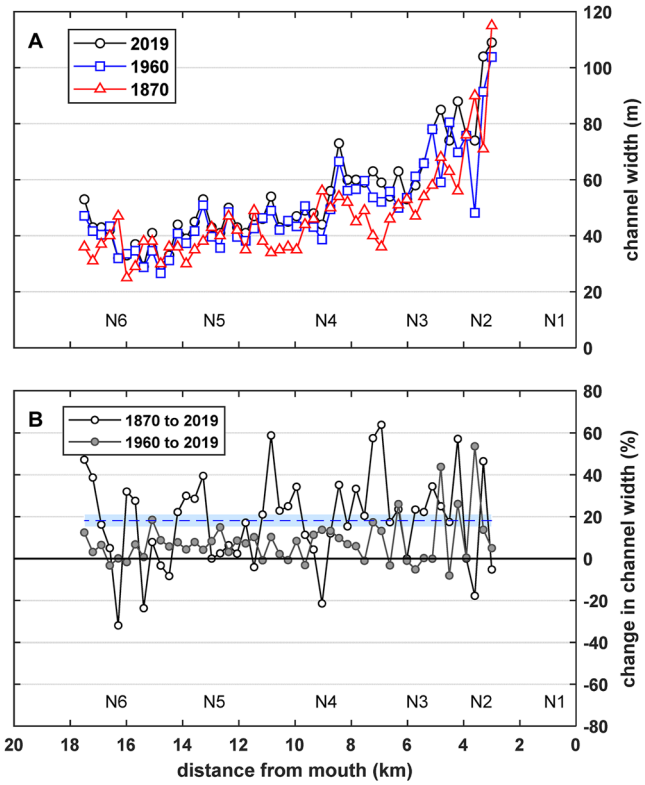

Figure 6. Panel (a) shows North River channel widths in 2019, 1960, and 1870 versus distance from the inlet. Panel (b) shows the percentage change in North River width from 1870 to 2019 (black) and from 1960 to 2019 (gray). Negative % values indicate narrowing, and positive % values indicate widening. The dashed blue line represents the average channel widening from 1870 to 2019. The shaded area represents the standard error of the mean. Note that distances from the ocean increase to the left, consistent with our site map.

lead accumulated at the surface of the relatively slowly building marsh platform, likely via the advection of detrital organic material onto which metals tend to adsorb (Lin & Chen, 1998). The foraminifera assemblage transition at N3C1 from one dominated by high marsh species (*J. macrescens* and *T. inflata*) just below the organic horizon at 70 cm depth to an assemblage with increased *M. fusca*, *Ammobaculites* spp. and *Reophax* spp. beginning just above the layer at 65 cm depth is consistent with a sudden increase in inundation due to the 1898 switch in inlet location. A similar change in foraminifera species assemblage was observed following an increase in tidal inundation due to removal of a tide gate in Oregon, USA (Milker et al., 2022). Specifically, the change in foraminifera assemblage supports a change in depositional environment from above MHW before the inlet switch to below MHW afterward. The foraminifera sample taken directly above the organic marker horizon at 65 cm depth contained an assemblage of species that are consistent with a mixing signature and sourcing from previously deposited reworked bank material. Following the inlet switch and resultant increase in MHW along the North River, sediment organic content abruptly decreased from 46% to 7% in core N3C1 (Figure 2a). The mineral-rich nature of this overlying sediment reflects a greater hydroperiod and inundation depth following the inlet switch (Roner et al., 2016; Temmerman et al., 2005).

Marsh sediment accretion rates at N3C1 over the first half of the 20th century (1898–1963) of 6 mm/yr were roughly four times the regional rate of SLR of 1.5 mm/yr during that time (Talke et al., 2018). Rapid accumulation rates in the early 1900s were initially supported largely through enhanced trapping of mineral sediment with 93% mineral content (7% LOI) observed just above the 1898 event layer. As the marsh built elevation over the ensuing decades, inundation depths and mineral sediment trapping decreased, which is reflected by the increase in LOI toward the core top. Some of the observed increasing LOI trend toward the surface may also be due to decomposition at depth. While sedimentation rates remained similar during the latter half of the record, averaging 6 mm/yr from 1963 to present, this was only twice the rate of SLR over the same time period of 3.0 mm/yr (Talke et al., 2018). Therefore, this reflects a deceleration in sedimentation relative to an increasing rate of SLR. For reference, the average accumulation rate for the last ~100 years at 10 other Massachusetts Bay marshes with well-constrained age models is 3.9 mm/yr (SD = 0.75 mm/yr), or 1.35 times the contemporaneous rate of SLR, with a maximum reported accumulation rate of 5.2 mm/yr (O'Keefe Suttles et al., 2021). Our surficial foraminiferal sample at N3 contained more than 50% *M. fusca*, which shows that the marsh has yet to aggrade sufficiently within the tidal frame to match inundation frequencies prior to the inlet switch. Furthermore, marsh inundation depths along the North River remain greater than those along the South River (Figure 5). Thus, the timescale of marsh adjustment for the North River system likely exceeds ~120 years.

Proximal to the new inlet, average sediment accumulation rates based on a ~1900 onset for bulk lead contamination have been even greater than that observed at N3, averaging 10 and 8 mm/yr respectively for N1 and N2. The high deposition rate at N1 is likely due to rapid subsidence providing accommodation space and abundant marine-derived sediment (Baranes et al., 2022). We hypothesize that the high subsidence rate at N1 was caused by rapid peat oxidation due to the dense channel network at N1 that allows for efficient drainage of the marsh peat.

By examining modern water levels, modern marsh platform elevation, and estimating average marsh compaction for the region, we can make an approximation of how platform elevation and water levels have adjusted since the 1898 inlet switch. For this analysis, we rely on observations from site N3, where field observations provide good estimates for modern elevations of MHW, the marsh platform, and the organic-rich marker horizon (Figure 7, 2018 panel). Based on observed modern MHW attenuation of 5 cm/km, we estimate that North River MHW increased in 1898 by a minimum of 30 cm following the 6 km channel shortening. Regional relative SLR since the inlet switch has also increased water levels, totaling 25 cm during 1898–2018 (Talke et al., 2018). SLR plus

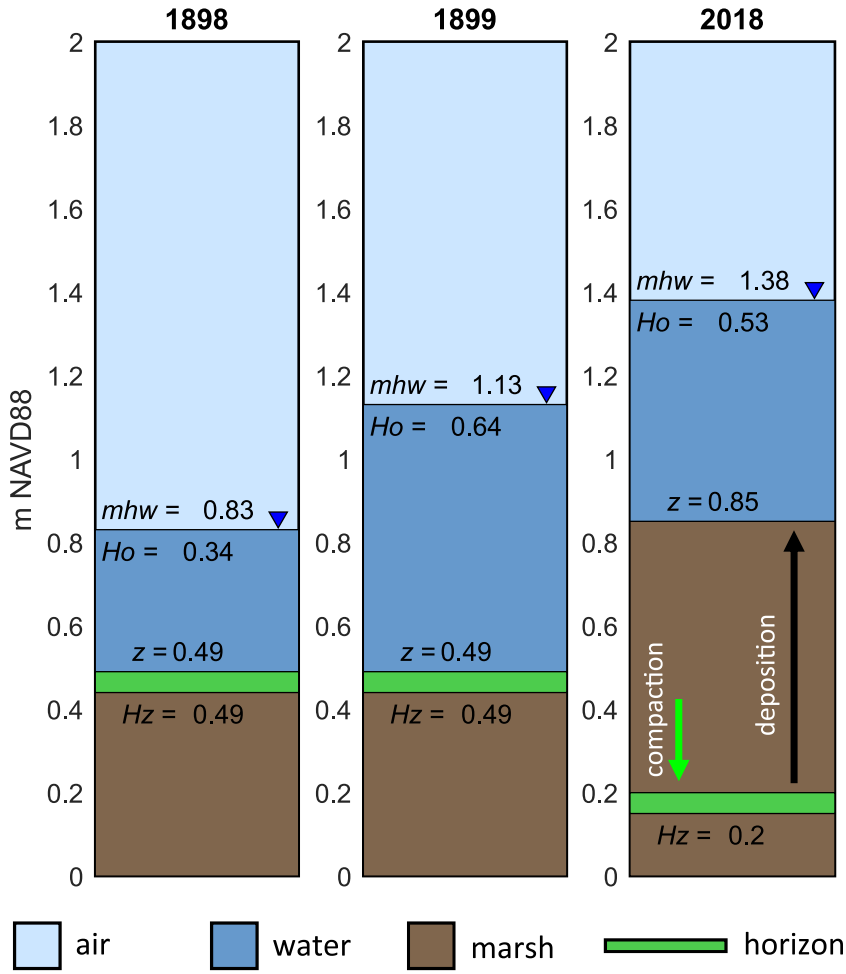

Figure 7. Schematic diagram of marsh platform and MHW elevations in meters relative to the NAVD88 datum through time at the site of our N3C1 core. Brown is marsh sediment, dark blue is water, and light blue is air. The green bar represents the 1898 marker horizon (see methods). The left panel depicts conditions just prior to the 1898 inlet switch. The middle panel, 1899, depicts conditions just after the inlet switch. The right panel, 2018, depicts conditions at the time of the study. Labels on the plots refer to elevations in m NAVD88, except for Ho. Label abbreviations are as follows: MHW = mean high water; z = platform elevation; Hz = top of the marker horizon; Ho = inundation depth (MHW-z).

the inlet switch-induced increase in MWH totals ~55 cm, which is 10 cm less than the 65 cm of sediment deposition at N3 during the same time (Figure 2). Marsh compaction explains the discrepancy of sediment deposition 10 cm in excess of the accommodation space provided by the increase in MHW levels. Compaction provided additional accommodation space by lowering the marsh platform during the 120 years following the inlet switch and loading of the marsh platform with mineral-rich sediment (Figure 7).

Compaction creates accommodation space between the marsh platform and MHW and can allow for deposition rates in excess of SLR (Brain et al., 2017; Cahoon et al., 2002). Using well-constrained age models from marsh cores from the region, we used the difference between sedimentation rates and SLR to estimate marsh compaction (Cahoon et al., 1995). Between 1898 and 2018 sea level rose 25 cm (Talke et al., 2018) and salt marsh deposition rates multiplied by 120 years at natural reference sites reported in O'Keefe Suttles et al. (2019) averaged 54 cm (n = 10, st.dev. = 9.0 cm). Excess sedimentation above SLR assuming a constant inundation depth through time yields a regional compaction estimate of ~30 cm. Following thin layer placement of mineral-rich dredge sediment, marshes have been observed to undergo enhanced compaction (VanZomeren et al., 2018). We therefore view our compaction calculation as a minimum estimate for N3, as increased mineral sediment deposition there following the inlet switch likely amplified loading. Based on this minimum autocompaction estimate, the 1898 marsh platform and marker horizon (green bar in Figure 7) was ~30 cm higher than present elevation at the time of the inlet

switch. This gradual compaction adjustment allows for the immediate increase in MWH after the inlet switch to persist to the modern in step with regional SLR. Persistent *Miliammina fusca* abundance within foraminiferal assemblages since the inlet switch through present day support this interpretation of continuously high inundation relative to pre-1898 conditions (Figure 4). A discrepancy still exists between pre-inlet switch estimated MHW inundation depth of 0.34 m and foraminiferal assemblages which suggest a platform elevation roughly equal to MHW. This discrepancy is likely due in part to the aforementioned conservative estimate of compaction, which was likely exceeded at N3. Furthermore, present day tidal attenuation may be less than occurred through the pre-1898 inlet, which was bounded by a prograding spit that constrained the channel. The new inlet is bounded by headlands and not impinged by a mobile spit, generally resulting in a much wider inlet relative to geometry of the old inlet, as depicted in the 1870 map (Figure 1). The more efficient new inlet helps explain the persistently high inundation depths since the inlet switch inferred from foraminifera. A steeper pre-1898 MHW attenuation gradient with distance from the inlet would have amplified the MWH increase following the inlet switch. This larger inferred increase in MHW would compel lower pre-1898 inundation at N3, consistent with foraminifera data that suggest infrequent inundation below the fibrous marker horizon.

The North River marsh's high accumulation rates provide an example of how a salt marsh can adjust to greater inundation depths when there is a sufficient mineral sediment supply. In general, the North-South Rivers Estuary is a mineral rich system. In the upper 50 cm of the marsh platform across core transects less than 12 km from the inlet, dry sediment subsamples averaged 76% mineral, versus 66% for other sites in the region (O'Keefe Suttles et al., 2021). At nearby Nauset Marsh (Cape Cod, Massachusetts, USA), sedimentation rates of up to 23.7 mm/y of largely mineral material were observed in response to the system's inlet migrating toward the measurement location (Roman et al., 1997). These rates were more than 10 times higher than those observed by Roman et al. (1997) at sites distal to the inlet site location. Were high temporal resolution observations available for the North River marsh in the early 1900s, we would expect similarly high accumulation rates immediately following the inlet switch at sites close to the new inlet.

Marshes along the South River channel were also affected by the inlet switch and resultant adjustment in water levels. Unlike the North River, South River MHW likely decreased in response to the inlet switch lengthening its channel by 5.6 km and nearly doubling the length of its tidal reach. Based on present day MHW attenuation of 5 cm/km, marsh inundation depths likely decreased by roughly 30 cm after the old inlet closed completely. The observed increase in LOI above the bulk lead onset (Figure 2), which we interpret as roughly coincident with the inlet switch, is consistent with decreased inundation in the South River marsh resulting in less mineral sediment delivery and a shift toward more organogenic conditions. South River marsh accumulation rates at S3 of 3.0 mm/yr during the last 100 years were slower than nine out of 10 reported marsh accumulation rates from the region (O'Keefe Suttles et al., 2021). The relatively slow sediment accumulation rates observed for the South River are likely due to reduced inundation depths and hydroperiods, which would have limited mineral material deposition (Temmerman et al., 2003). Furthermore, lengthening of the South River channel due to the closing of the old inlet would have decreased delivery of marine sediment, the system's primary mineral sediment source (Baranes et al., 2022).

Silt-peat transitions in marsh sediment have been interpreted as largely the product of local engineering projects or large-scale forcing such as changes in SLR or seismically-induced subsidence (Allen, 1997). Here we show that inlet dynamics that affect the propagation of tides may cause similar changes in lithology through stratigraphic sections. Presently, marsh elevations relative to MHW are similar along the North and South Rivers at corresponding distances from the inlet, suggesting that the system has moved toward equilibrium with respect to the 1898 disturbance (Figure 5). Increased mineral sediment accumulation following the inlet switch was likely in part due to increased hydroperiod (Allen, 2000; Temmerman et al., 2003), but it is also likely that sediment concentrations increased in the North River after the inlet switch. The opening of the new inlet through the beach between two prominent bluffs comprised of glacial till, which has abundant clay and silts (Yellen et al., 2016) exposed these deposits to enhanced erosion that likely supplied fine grained mineral material to the North River marsh. Furthermore, the increased tidal prism within the North River channel network caused by the increase in MHW widened its channel, with eroded bank material providing an additional source of sediment. The mixed foraminiferal assemblage of low and high marsh foraminifera found immediately above the fibrous high marsh sediment supports rapid bank erosion as a source of sediment to the marsh platform, which has been documented in the region (Hopkinson et al., 2018).

5.2. Tidal Elevations and Marsh Morphology

Modern MHW elevations decrease up-estuary at similar rates within the two main channels of the estuary, suggesting that the balance between channel friction and inertial forces within this system is roughly equivalent between the two main channels. This balance between dissipative and momentum forces in convergent estuarine channels, defined as those whose width decreases in the landward direction, is well documented in theoretical discussion (Fagherazzi & Furbish, 2001; Green, 1838; Jay, 1991; Lanzoni & Seminara, 1998). Our observations of decreasing landward MHW indicate that the North and South Rivers constitute a strongly dissipative system. The slight increase in MHW at our most landward site (N6) is likely the result of partial reflection of the tidal wave near the head of the estuary.

Carefully surveyed historical maps as far back as 1870 (Gannett & Grambs, 1888; Peirce et al., 1870) indicate that channel locations have been relatively stable with the exception of the inlet switch. Aerial imagery from 1951 (University of Massachusetts, 1952) confirms stable channel dimensions since the mid-20th century. We therefore assume that pre-1898 up-estuary MHW attenuation occurred at a similar rate. Based on this assumption, the 5.6 km shortening of the North River channel would have caused, at minimum, a MHW increase of roughly 30 cm, which is equivalent to present day total inundation depths at site S3 and S4. We consider this a minimum value due to the more efficient modern inlet versus the smaller, spit-bound old inlet. Firsthand accounts support this interpretation of an instantaneous increase in MHW along the North River. For example, *S. alterniflora* replaced *S. patens* along North River marshes, and the North River Boat Club house (river km 6.5) had to be moved due to regular flooding immediately following the inlet switch (Freitas & Ball, 1995). Furthermore, an Atlantic white cedar stand located just upstream of N5 (42.112714, −70.779918) died following the inlet switch, consistent with higher water levels drowning these trees (F. Freitas, personal communication, 2021). The platform morphology of the estuary's marshes, which is common to this region (FitzGerald & Hughes, 2019), dictates that any change in tidal propagation over the marsh will have a disproportionate impact on tidal prism volume and resultant tidal velocities. North River marshes comprise roughly two thirds of the total estuarine area, and therefore, the increase in North River marsh inundation would have dramatically increased the tidal prism. We attribute the increase in North River channel widths (Figure 6) to erosion associated with channel adjustments to accommodate this increase in tidal prism.

Elsewhere in the region, channel widening has been attributed to crab herbivory (Smith, 2009) and 20th century SLR acceleration (Watson et al., 2017). In the case of the North and South Rivers, it is likely that the inlet switch and resultant changes in tidal range has driven the changes in channel dimensions. Namely, the North River widened and the South River did not. Channel dimensions are still responding to the inlet switch-altered tidal prisms. The rate of North River widening suggested by the comparison of 1870, 1960, and 2019 channel widths was relatively constant during pre versus post 1960 periods (Figure 6), suggesting continued channel widening to present. Along the North River channel banks, we observed marsh strata that are tilted downwards toward the channel that likely indicate slumping due to erosion and/or oxidation of the underlying sediments (see photo, Figure S1 in Supporting Information S1). The organic-rich 1898 marker horizon slopes toward the channel within 10 m of the bank, providing further evidence for slumping (Figure S4 in Supporting Information S1). The widening of the North River channel during 1870–2019 represents horizontal erosion of the marsh platform. Using the reach lengths, change in channel width, and an average bank height of 3 m, we estimated the total eroded volume of marsh soil equaled 330,000 m^3. If this sediment were redistributed equally across the entire area of the present-day North River marsh platform assuming a similar bulk density of the eroded and deposited material, it would account for 6–8 cm of deposition, or ∼10% of deposition since the inlet switch. Thus, internal sources of material played a minor role in allowing the marsh to aggrade rapidly, and an external source is required to account for a majority of mineral sediment that has accumulated on the marsh since 1898. Results presented in Baranes et al. (2022) and here in Figure 3 provide support for marine-derived sediment as this dominant source.

In contrast to the North River, we hypothesize that the South River's cross sectional area decreased following the 1898 inlet switch resulting in a reduction in tidal prism on the South River. Although repeat width measurements from historical maps and photos did not indicate narrowing of the channel, we suggest that shallowing has allowed for reduction in South River channel cross sectional area. Visible sandy shoals in the South River channel in 2014 aerial photos provide evidence for this adjustment (Figure S6 in Supporting Information S1). Recent topo-bathy lidar for the system (NOAA, 2022) reveals an average thalweg elevation of −0.7 m NAVD88 for the North River versus −0.3 m NAVD88 for the South River (extracted from each channel within river km

5–10 where the channels are not bound by hard substrate). The shallower depth of the South River relative to the North River is consistent with bed aggradation on the South River allowing for adjustment to a smaller post-1898 tidal prism.

5.3. Implications for Marsh Resilience

Despite the stress of increased inundation after the 1898 inlet switch, marshes along the North River channel have been resilient based on the US Geological Survey's widely applied metric for marsh health, the unvegetated to vegetated ratio (UVVR) (Ganju et al., 2022). Area weighted UVVR for the North River marshes averages 0.17, which falls in line with average UVVR for healthy marshes (Ganju et al., 2017). Observations presented here that show the conditions that allowed for this marsh's resilience have implications for effective marsh management, as well as the beaches that front them. With respect to beaches, we illustrate that inlet location can be a first order control in modulating local tidal heights, with the ∼30 cm MHW increase from inlet switch equaling or exceeding the magnitude of relative SLR at this location for the preceding century. Thus, it is worth emphasizing that variations in tidal range caused by dredging (e.g., Ralston et al., 2019), changes in inlet location, or channel straightening, can have larger short term impacts on marshes than regional or global SLR trends. With respect to marshes, the 1898 rapid increase in North River MHW provides an example of greater inundation allowing for increased delivery of mineral sediment (Mudd et al., 2009; Temmerman et al., 2003). It is likely that generally high sediment loads from coastal erosion of fine-grained glacial deposits following the inlet switch in part allowed for this rapid adjustment. As mentioned earlier, similar observations of marsh resilience to rapid relative SLR caused by groundwater withdrawals have been observed when coupled with abundant mineral sediment supply (Watson, 2004). However, in an example of increased inundation at the more sediment limited Ni-les'tun marsh in Oregon, USA, removal of a tidal gate resulted in a ∼1 m increase in marsh inundation depths, but sedimentation rates in the first 5 years were only 3 mm/yr (Horton et al., 2017).

In addition to abundant sediment supplies provided in part by glacial legacy sediments at the new inlet, marsh systems that formed behind barrier beach systems depend on the stability of the beach location to persist. The North-South Rivers Estuary barrier beach is anchored in part by slowly eroding headlands (drumlins) that help to stabilize the beach location, which otherwise would likely be transgressing. Marsh vertical accretion can play a dominant role in marsh persistence when steep uplands prevent landward migration, but only provided an external suspended sediment supply.

If marshes are to survive rapid SLR, especially in sediment-deficient regions like the Northeast US, we need to ensure that marshes have continued access to mineral sediment supplies. Removing sediment from estuarine systems, for example, via dredging, presents an added stressor (Chant et al., 2021; Ganju, 2019) that compounds the effects of accelerating SLR and eutrophication (Deegan et al., 2012; Turner et al., 2009; Wigand et al., 2014). Similarly, engineering of the coastline to halt erosion may have the unintended consequence of reducing sources of sediment important to marsh health (Baranes et al., 2022; Hache et al., 2020; Peteet et al., 2018). In coastal regions that lack large supplies of suspended fluvial sediment, such as the coastlines of the northeast US, Australia, and West Africa (Milliman & Farnsworth, 2013), managers must consider alternate supplies of sediment to replace the potentially reduced sediment flux from armored coastlines and dredging projects.

6. Conclusion

A change in inlet location to the North-South Rivers Estuary during the 1898 Portland Gale caused an abrupt ∼30 cm increase in mean high water along the shortened North River, illustrating the role of barrier dynamics in modulating tidal inundation depths in salt marshes. The increase in tidal heights provided an opportunity to observe resultant changes to tidal marsh lithology and elevation under conditions analogous to rapid SLR. North River tidal marshes proved resilient to increased inundation, rapidly building elevation at up to five times the rate of regional SLR over the same time period. Initially, rapid accumulation of inorganic material played a large role in building elevation, providing evidence that mesotidal marshes with sufficient supplies of mineralogic sediment should be resilient to projected future SLR. Dredging and shoreline armoring currently reduce marine sediment which is the main supply of sediment to many tidal marshes in the Northeast US, where sediment loads from local rivers are generally low. Therefore, in order to build tidal marsh resilience, management efforts should be focused on creative solutions that restore sediment sources that are lost to dredging and shoreline armoring.

Conflict of Interest

The authors declare no conflicts of interest relevant to this study.

Data Availability Statement

The NOAA Tidal Analysis Datums Calculator software is available here: https://access.co-ops.nos.noaa.gov/datumcalc/. Tidal marsh and channel observations are available here: https://doi.org/10.7275/szte-xm56.

Acknowledgments
The project described in this publication was in part supported by Grant or Cooperative Agreement No. G20AC00071 from the U.S. Geological Survey and a Department of Interior Northeast Climate Adaptation Science Center graduate fellowship awarded to H.E.B and B.C.Y. (G12AC00001). Its contents are solely the responsibility of the authors and do not necessarily represent views of the Northeast Climate Adaptation Science Center or the USGS. A special thanks to A. DiTroia, D. Beach, B. Jette, C. Ladlow and J. Sisson for help in fieldwork and lab analyses. J.D.W. did initial analyses for this publication while in residency at the Darling Marine Center. David Ball and Fred Frietas of Scituate, MA provided useful guidance on historical accounts of the 1898 Portland Gale.

References

Allen, J. R. L. (1997). Simulation models of salt-marsh morphodynamics: Some implications for high-intertidal sediment couplets related to sea-level change. *Sedimentary Geology*, *113*(3–4), 211–223. https://doi.org/10.1016/S0037-0738(97)00101-2

Allen, J. R. L. (2000). Morphodynamics of Holocene salt marshes: A review sketch from the Atlantic and Southern North Sea coasts of Europe. *Quaternary Science Reviews*, *19*(12), 1155–1231. https://doi.org/10.1016/S0277-3791(99)00034-7

Anisfeld, S. C., Tobin, M. J., & Benoit, G. (1999). Sedimentation rates in flow-restricted and restored salt marshes in Long Island Sound. *Estuaries*, *22*(2), 231. https://doi.org/10.2307/1352980

Atwater, B., & Hemphill-Haley, E. (1996). *Preliminary estimates of recurrence intervals for great earthquakes of the past 3500 years at Northeastern Willapa Bay, Washington (no. open-file report 96-001)*. U.S. Geological Survey.

Aykut, N. O., Gulal, E., & Akpinar, B. (2015). Performance of single base RTK GNSS method versus network RTK. *Earth Sciences Research Journal*, *19*(2), 135–139. https://doi.org/10.15446/esrj.v19n2.51218

Baranes, H. E., Woodruff, J. D., Geyer, W. R., Yellen, B. C., Richardson, J. B., & Griswold, F. (2022). Sources, mechanisms, and timescales of sediment delivery to a New England Salt Marsh. *Journal of Geophysical Research: Earth Surface*, *127*(3), e2021JF006478. https://doi.org/10.1029/2021JF006478

Boldt, K. V., Lane, P., Woodruff, J. D., & Donnelly, J. P. (2010). Calibrating a sedimentary record of overwash from Southeastern New England using modeled historic hurricane surges. *Marine Geology*, *275*(1–4), 127–139. https://doi.org/10.1016/j.margeo.2010.05.002

Boumans, R. M. J., Burdick, D. M., & Dionne, M. (2002). Modeling habitat change in salt marshes after tidal restoration. *Restoration Ecology*, *10*(3), 543–555. https://doi.org/10.1046/j.1526-100X.2002.02032.x

Brain, M. J., Kemp, A. C., Hawkes, A. D., Engelhart, S. E., Vane, C. H., Cahill, N., et al. (2017). Exploring mechanisms of compaction in salt-marsh sediments using Common Era relative sea-level reconstructions. *Quaternary Science Reviews*, *167*, 96–111. https://doi.org/10.1016/j.quascirev.2017.04.027

Bricker-Urso, S., Nixon, S. W., Cochran, J. K., Hirschberg, D. J., & Hunt, C. (1989). Accretion rates and sediment accumulation in Rhode Island salt marshes. *Estuaries*, *12*(4), 300–317. https://doi.org/10.2307/1351908

Buynevich, I. V., & Donnelly, J. P. (2006). Geological signatures of barrier breaching and overwash, southern Massachusetts, USA. *Journal of Coastal Research*, *39*, 112–116.

Cahoon, D. R., Lynch, J. C., Perez, B. C., Segura, B., Holland, R. D., Stelly, C., et al. (2002). High-precision measurements of wetland sediment elevation: II. The Rod surface elevation table. *Journal of Sedimentary Research*, *72*(5), 734–739. https://doi.org/10.1306/020702720734

Cahoon, D. R., Lynch, J. C., Roman, C. T., Schmit, J. P., & Skidds, D. E. (2019). Evaluating the relationship among wetland vertical development, elevation Capital, sea-level rise, and tidal marsh Sustainability. *Estuaries and Coasts*, *42*, 1–15. https://doi.org/10.1007/s12237-018-0448-x

Cahoon, D. R., Reed, D. J., & Day, J. W. (1995). Estimating shallow subsidence in microtidal salt marshes of the southeastern United States: Kaye and Barghoorn revisited. *Marine Geology*, *128*(1–2), 1–9. https://doi.org/10.1016/0025-3227(95)00087-F

Chant, R. J., Ralston, D. K., Ganju, N. K., Pianca, C., Simonson, A. E., & Cartwright, R. A. (2021). Sediment budget estimates for a highly impacted embayment with extensive wetland loss. *Estuaries and Coasts*, *44*(3), 608–626. https://doi.org/10.1007/s12237-020-00784-3

Coleman, D. J., Schuerch, M., Temmerman, S., Guntenspergen, G., Smith, C. G., & Kirwan, M. L. (2022). Reconciling models and measurements of marsh vulnerability to sea level rise. *Limnology and Oceanography Letters*, *7*(2), 140–149. https://doi.org/10.1002/lol2.10230

Cook, T. L., Yellen, B. C., Woodruff, J. D., & Miller, D. (2015). Contrasting human versus climatic impacts on erosion. *Geophysical Research Letters*, *42*(16), 6680–6687. https://doi.org/10.1002/2015GL064436

Crosby, S. C., Sax, D. F., Palmer, M. E., Booth, H. S., Deegan, L. A., Bertness, M. D., & Leslie, H. M. (2016). Salt marsh persistence is threatened by predicted sea-level rise. *Estuarine, Coastal and Shelf Science*, *181*, 93–99. https://doi.org/10.1016/j.ecss.2016.08.018

Croudace, I. W., Rindby, A., & Rothwell, R. G. (2006). ITRAX: Description and evaluation of a new multi-function X-ray core scanner. *Geological Society, London, Special Publications*, *267*(1), 51–63. https://doi.org/10.1144/gsl.sp.2006.267.01.04

Cundy, A. B., & Croudace, I. W. (1996). Sediment accretion and recent sea-level rise in the Solent, southern England: Inferences from radiometric and geochemical studies. *Estuarine, Coastal and Shelf Science*, *43*(4), 449–467. https://doi.org/10.1006/ecss.1996.0081

D'Alpaos, A., Lanzoni, S., Marani, M., & Rinaldo, A. (2007). Landscape evolution in tidal embayments: Modeling the interplay of erosion, sedimentation, and vegetation dynamics. *Journal of Geophysical Research*, *112*(F1), F01008. https://doi.org/10.1029/2006JF000537

Day, J. W., Rybczyk, J., Scarton, F., Rismondo, A., Are, D., & Cecconi, G. (1999). Soil accretionary dynamics, sea-level rise and the survival of wetlands in Venice Lagoon: A field and modelling approach. *Estuarine, Coastal and Shelf Science*, *49*(5), 607–628. https://doi.org/10.1006/ecss.1999.0522

Dean, W. E. (1974). Determination of carbonate and organic matter in calcareous sediments and sedimentary rocks by loss on ignition; comparison with other methods. *Journal of Sedimentary Research*, *44*, 242–248.

Deegan, L. A., Johnson, D. S., Warren, R. S., Peterson, B. J., Fleeger, J. W., Fagherazzi, S., & Wollheim, W. M. (2012). Coastal eutrophication as a driver of salt marsh loss. *Nature*, *490*(7420), 388–392. https://doi.org/10.1038/nature11533

Doyle, T. W., Krauss, K. W., Conner, W. H., & From, A. S. (2010). Predicting the retreat and migration of tidal forests along the northern Gulf of Mexico under sea-level rise. *Forest Ecology and Management*, *259*(4), 770–777. https://doi.org/10.1016/j.foreco.2009.10.023

Emery, K. O., Wigley, R. L., & Rubin, M. (1965). A Submerged peat deposit off the Atlantic coast of the United States 1. *Limnology & Oceanography*, *10*(suppl), R97–R102. https://doi.org/10.4319/lo.1965.10.suppl2.r97

Fagherazzi, S., Anisfeld, S. C., Blum, L. K., Long, E. V., Feagin, R. A., Fernandes, A., et al. (2019). Sea level rise and the dynamics of the marsh-upland boundary. *Frontiers in Environmental Science*, *7*, 25. https://doi.org/10.3389/fenvs.2019.00025

Fagherazzi, S., & Furbish, D. J. (2001). On the shape and widening of salt marsh creeks. *Journal of Geophysical Research*, *106*(C1), 991–1003. https://doi.org/10.1029/1999JC000115

Fagherazzi, S., Kirwan, M. L., Mudd, S. M., Guntenspergen, G. R., Temmerman, S., D'Alpaos, A., et al. (2012). Numerical models of salt marsh evolution: Ecological, geomorphic, and climatic factors. *Reviews of Geophysics*, *50*(1), RG1002. https://doi.org/10.1029/2011RG000359

Filipescu, S., & Kaminski, M. A. (2011). Re-discovering Entzia, an agglutinated foraminifer from the Transylvanian salt marshes. In *Proceedings of the eighth international workshop on agglutinated foraminifera* (pp. 29–35). Grzybowski Foundation Special Publication.

FitzGerald, D., Ryerson, O., Hughes, Z., Black, S., Georgiou, I., Hein, C., & Novak, A. (2020). Long-term variability in inorganic sediment contributions to the Great Marsh, Massachusetts. *Journal of Coastal Research*, *95*(sp1), 490–494. https://doi.org/10.2112/SI95-095.1

FitzGerald, D. M. (1988). Shoreline erosional-depositional processes associated with tidal inlets. In D. G. Aubrey & L. Weishar (Eds.), *Hydrodynamics and sediment dynamics of tidal inlets, lecture notes on coastal and estuarine studies* (pp. 186–225). Springer. https://doi.org/10.1007/978-1-4757-4057-8_11

FitzGerald, D. M., & Hughes, Z. (2019). Marsh processes and their response to climate change and sea-level rise. *Annual Review of Earth and Planetary Sciences*, *47*(1), 481–517. https://doi.org/10.1146/annurev-earth-082517-010255

FitzGerald, D. M., & Pendleton, E. (2002). Inlet formation and evolution of the sediment bypassing system: New Inlet, Cape Cod, Massachusetts. *Journal of Coastal Research*, *36*, 290–299. https://doi.org/10.2112/1551-5036-36.sp1.290

Freitas, F., & Ball, D. (1995). Warnings Ignored! The Story of The Portland Gale November, 1898. Converpage, Scituate Massachusetts.

French, J. (2006). Tidal marsh sedimentation and resilience to environmental change: Exploratory modelling of tidal, sea-level and sediment supply forcing in predominantly allochthonous systems. *Marine Geology*, *235*(1–4), 119–136. https://doi.org/10.1016/j.margeo.2006.10.009

Friedrichs, C. T., & Perry, J. E. (2001). Tidal salt marsh morphodynamics: A Synthesis. *Journal of Coastal Research*, *27*, 7–37.

Ganju, N. K. (2019). Marshes are the new beaches: Integrating sediment transport into restoration planning. *Estuaries and Coasts*, *42*(4), 917–926. https://doi.org/10.1007/s12237-019-00531-3

Ganju, N. K., Couvillion, B. R., Defne, Z., & Ackerman, K. V. (2022). Development and application of landsat-based wetland vegetation cover and unvegetated-vegetated marsh ratio (UVVR) for the conterminous United States. *Estuaries and Coasts*, *45*(7), 1861–1878. https://doi.org/10.1007/s12237-022-01081-x

Ganju, N. K., Defne, Z., Kirwan, M. L., Fagherazzi, S., D'Alpaos, A., & Carniello, L. (2017). Spatially integrative metrics reveal hidden vulnerability of microtidal salt marshes. *Nature Communications*, *8*, 1–7. https://doi.org/10.1038/ncomms14156

Gannett, H., & Grambs, W. J. (1888). *Massachusetts—Duxbury sheet*. USGS Topographic Maps.

Green, G. (1838). On the motion of waves in a variable canal of small depth and width. *Transactions of the Cambridge Philosophical Society*, *6*, 457.

Hache, I., Karius, V., & von Eynatten, H. (2020). Suspended particulate matter for sediment accumulation on inundated anthropogenic marshland in the southern North Sea—Potential, thresholds and limitations. *Continental Shelf Research*, *207*, 104214. https://doi.org/10.1016/j.csr.2020.104214

Hayes, M. O. (1979). Barrier island morphology as a function of tidal and wave regime. In S. P. Leatherman (Ed.), *Barrier islands* (Vol. 1, 27). Academic Press.

Hayes, M. O., & FitzGerald, D. M. (2013). Origin, evolution, and classification of tidal inlets. *Journal of Coastal Research*, *69*, 14–33. https://doi.org/10.2112/SI_69_3

Hein, C. J., FitzGerald, D. M., Carruthers, E. A., Stone, B. D., Barnhardt, W. A., & Gontz, A. M. (2012). Refining the model of barrier island formation along a paraglacial coast in the Gulf of Maine. *Marine Geology*, *307*(310), 40–57. https://doi.org/10.1016/j.margeo.2012.03.001

Hopkinson, C. S., Morris, J. T., Fagherazzi, S., Wollheim, W. M., & Raymond, P. A. (2018). Lateral marsh edge erosion as a source of sediments for vertical marsh accretion. *Journal of Geophysical Research: Biogeosciences*, *123*(8), 2444–2465. https://doi.org/10.1029/2017JG004358

Horton, B. P., Khan, N. S., Cahill, N., Lee, J. S. H., Shaw, T. A., Garner, A. J., et al. (2020). Estimating global mean sea-level rise and its uncertainties by 2100 and 2300 from an expert survey. *Npj Climate and Atmospheric Science*, *3*, 1–8. https://doi.org/10.1038/s41612-020-0121-5

Horton, B. P., Milker, Y., Dura, T., Wang, K., Bridgeland, W. T., Brophy, L., et al. (2017). Microfossil measures of rapid sea-level rise: Timing of response of two microfossil groups to a sudden tidal-flooding experiment in Cascadia. *Geology*, *45*(6), 535–538. https://doi.org/10.1130/G38832.1

Italiani, D., Siegle, E., & Noernberg, M. A. (2020). Tidal inlet migration and formation: The case of the Ararapira inlet-Brazil. *Ocean and Coastal Research*, *68*, e20314. https://doi.org/10.1590/S2675-28242020068314

Jay, D. A. (1991). Green's law revisited: Tidal long-wave propagation in channels with strong topography. *Journal of Geophysical Research*, *96*(C11), 20585–20598. https://doi.org/10.1029/91JC01633

Kemp, A. C., Hawkes, A. D., Donnelly, J. P., Vane, C. H., Horton, B. P., Hill, T. D., et al. (2015). Relative sea-level change in Connecticut (USA) during the last 2200 yrs. *Earth and Planetary Science Letters*, *428*, 217–229. https://doi.org/10.1016/j.epsl.2015.07.034

Kemp, A. C., Wright, A. J., & Cahill, N. (2020). Enough is enough, or more is more? Testing the influence of foraminiferal count size on reconstructions of paleo-marsh elevation. *Journal of Foraminiferal Research*, *50*(3), 266–278. https://doi.org/10.2113/gsjfr.50.3.266

Kirwan, M. L., & Guntenspergen, G. R. (2010). Influence of tidal range on the stability of coastal marshland. *Journal of Geophysical Research*, *115*(F2), F02009. https://doi.org/10.1029/2009JF001400

Kirwan, M. L., & Guntenspergen, G. R. (2015). Response of plant productivity to experimental flooding in a stable and a submerging marsh. *Ecosystems*, *18*(5), 903–913. https://doi.org/10.1007/s10021-015-9870-0

Kolker, A. S., Allison, M. A., & Hameed, S. (2011). An evaluation of subsidence rates and sea-level variability in the northern Gulf of Mexico. *Geophysical Research Letters*, *38*(21), 21404. https://doi.org/10.1029/2011GL049458

Langston, A. K., Durán Vinent, O., Herbert, E. R., & Kirwan, M. L. (2020). Modeling long-term salt marsh response to sea level rise in the sediment-deficient Plum Island Estuary, MA. *Limnology & Oceanography*, *65*(9), 2142–2157. https://doi.org/10.1002/lno.11444

Lanzoni, S., & Seminara, G. (1998). On tide propagation in convergent estuaries. *Journal of Geophysical Research*, *103*(C13), 30793–30812. https://doi.org/10.1029/1998JC900015

Lin, J.-G., & Chen, S.-Y. (1998). The relationship between adsorption of heavy metal and organic matter in river sediments. *Environment International*, *24*(3), 345–352. https://doi.org/10.1016/S0160-4120(98)00012-9

Lucke, J. B. (1934). A theory of evolution of lagoon deposits on shorelines of emergence. *The Journal of Geology*, *42*(6), 561–584. https://doi.org/10.1086/624214

MassGIS. (2019). MassGIS data: 2019 Aerial imagery. Retrieved from https://www.mass.gov/info-details/massgis-data-2019-aerial-imagery#production

McKeon, K., Woodruff, J. D., Yellen, B., Fernald, S. H., & Sheehan, M. C. (2022). Invasive water chestnut hinders tidal wetland development. *Earth Surface Processes and Landforms*, *47*(6), 1409–1424. https://doi.org/10.1002/esp.5323

Meier, D. (2004). Man and environment in the marsh area of Schleswig–Holstein from Roman until late Medieval times. *Quaternary International*, *112*(1), 55–69. https://doi.org/10.1016/S1040-6182(03)00065-X

Milker, Y., Dura, T., & Horton, B. P. (2022). The response of foraminifera to rapid sea-level rise from tidal restoration of Ni-les'tun marsh, Oregon, USA. *Marine Geology*, *445*, 106757. https://doi.org/10.1016/j.margeo.2022.106757

Milliman, J. D., & Farnsworth, K. L. (2013). *River discharge to the coastal ocean: A global synthesis*. Cambridge University Press.

Morris, J. T., Sundareshwar, P. V., Nietch, C. T., Kjerfve, B., & Cahoon, D. R. (2002). Responses of coastal wetlands to rising sea level. *Ecology*, *83*(10), 2869–2877. https://doi.org/10.1890/0012-9658(2002)083[2869:ROCWTR]2.0.CO;2

Morton, R., Bernier, J., Barras, J., & Ferina, N. (2005). *Rapid subsidence and historical wetland loss in the Mississippi delta plain: Likely causes and future implications (no. open-file report 2005–1216)*. US GEological Survey.

Moskalski, S. M., & Sommerfield, C. K. (2012). Suspended sediment deposition and trapping efficiency in a Delaware salt marsh. *Geomorphology*, *139–140*, 195–204. https://doi.org/10.1016/j.geomorph.2011.10.018

Mudd, S. M., Howell, S. M., & Morris, J. T. (2009). Impact of dynamic feedbacks between sedimentation, sea-level rise, and biomass production on near-surface marsh stratigraphy and carbon accumulation. *Estuarine, Coastal and Shelf Science*, *82*(3), 377–389. https://doi.org/10.1016/j.ecss.2009.01.028

National Wetlands Inventory. (2013). US Fish and Wildlife Service, 2010. National Wetlands Inventory (WWW document). Retrieved from https://www.fws.gov/program/national-wetlands-inventory

NOAA. (2022). Topobathymetric Model for the New England Region States of New York, Connecticut, Rhode Island, and Massachusetts, 1887 to 2016.

O'Brien, M. P. (1969). Equilibrium flow areas of inlets on sandy coasts. *Journal of the Waterways and Harbors Division*, *95*(1), 43–52. https://doi.org/10.1061/JWHEAU.0000622

O'Keefe Suttles, J. A., Brosnahan, S. M., Gonneea, M. E., & Kroeger, K. D. (2019). Continuous monitoring data from natural and restored salt marshes on Cape Cod, Massachusetts, 2016–17: U.S. Geological Survey Data Release. https://doi.org/10.5066/P9YLXOY8

O'Keefe Suttles, J. A., Eagle, M. J., Mann, A. C., Spivak, A., Sanks, K., Daniel, R., & Kroeger, K. D. (2021). Collection, analysis, and age-dating of sediment cores from natural and restored salt marshes on Cape Cod, Massachusetts, 2015–2016. https://doi.org/10.5066/P9R154DY

Payne, A. R., Burdick, D. M., & Moore, G. E. (2019). Potential effects of sea-level rise on salt marsh elevation dynamics in a New Hampshire estuary. *Estuaries and Coasts*, *42*(6), 1405–1418. https://doi.org/10.1007/s12237-019-00589-z

Peck, E. K., Wheatcroft, R. A., & Brophy, L. S. (2020). Controls on sediment accretion and blue carbon burial in tidal saline wetlands: Insights from the Oregon coast, USA. *Journal of Geophysical Research: Biogeosciences*, *125*(2), e2019JG005464. https://doi.org/10.1029/2019JG005464

Pederson, D. C., Peteet, D. M., Kurdyla, D., & Guilderson, T. (2005). Medieval warming, Little Ice Age, and European impact on the environment during the last millennium in the lower Hudson Valley, New York, USA. *Quaternary Research*, *63*(3), 238–249. https://doi.org/10.1016/j.yqres.2005.01.001

Peirce, B., Whiting, H. L., & Tittman, O. H. (1870). *Sketch of North River, Mass*. U.S. Coast Survey.

Pennington, W., Cambray, R. S., Eakins, J. D., & Harkness, D. D. (1976). Radionuclide dating of the recent sediments of Blelham Tarn. *Freshwater Biology*, *6*(4), 317–331. https://doi.org/10.1111/j.1365-2427.1976.tb01617.x

Pennington, W., Tutin, T. G., Cambray, R. S., & Fisher, E. M. (1973). Observations on lake sediments using fallout 137Cs as a tracer. *Nature*, *242*(5396), 324–326. https://doi.org/10.1038/242324a0

Peteet, D. M., Nichols, J., Kenna, T., Chang, C., Browne, J., Reza, M., et al. (2018). Sediment starvation destroys New York City marshes' resistance to sea level rise. *Proceedings of the National Academy of Sciences of the United States of America*, *115*(41), 10281–10286. https://doi.org/10.1073/pnas.1715392115

Ralston, D., Yellen, B., & Woodruff, J. (2020). Watershed sediment supply and potential impacts of dam removals for an estuary.

Ralston, D. K., Talke, S., Geyer, W. R., Al-Zubaidi, H. A. M., & Sommerfield, C. K. (2019). Bigger tides, less flooding: Effects of dredging on barotropic dynamics in a highly modified estuary. *Journal of Geophysical Research: Oceans*, *124*(1), 196–211. https://doi.org/10.1029/2018JC014313

Rampino, M. R., & Sanders, J. E. (1980). Holocene transgression in south-central Long Island, New York. *Journal of Sedimentary Research*, *50*, 1063–1079. https://doi.org/10.1306/212F7B7B-2B24-11D7-8648000102C1865D

Redfield, A. C. (1972). Development of a New England salt marsh. *Ecological Monographs*, *42*(2), 201–237. https://doi.org/10.2307/1942263

Reed, D. J. (1990). The impact of sea-level rise on coastal salt marshes. *Progress in Physical Geography*, *14*(4), 465–481. https://doi.org/10.1177/030913339001400403

Roman, C. T., Peck, J. A., Allen, J. R., King, J. W., & Appleby, P. G. (1997). Accretion of a New England (U.S.A.) salt marsh in response to inlet migration, storms, and sea-level rise. *Estuarine, Coastal and Shelf Science*, *45*(6), 717–727. https://doi.org/10.1006/ecss.1997.0236

Roner, M., D'Alpaos, A., Ghinassi, M., Marani, M., Silvestri, S., Franceschinis, E., & Realdon, N. (2016). Spatial variation of salt-marsh organic and inorganic deposition and organic carbon accumulation: Inferences from the Venice lagoon, Italy. In *Advances in water resources, ecogeomorphological feedbacks of water fluxes, sediment transport and vegetation dynamics in rivers and estuaries* (Vol. *93*, pp. 276–287). https://doi.org/10.1016/j.advwatres.2015.11.011

Schönfeld, J., & Mendes, I. (2022). Benthic foraminifera and pore water carbonate chemistry on a tidal flat and salt marsh at Ria Formosa, Algarve, Portugal. *Estuarine, Coastal and Shelf Science*, *276*, 108003. https://doi.org/10.1016/j.ecss.2022.108003

Scott, D. B., & Medioli, F. S. (1980). Living vs. total foraminiferal populations: Their relative usefulness in paleoecology. *Journal of Paleontology*, *54*, 814–831.

Scott, D. S., & Medioli, F. S. (1978). Vertical zonations of marsh foraminifera as accurate indicators of former sea-levels. *Nature*, *272*(5653), 528–531. https://doi.org/10.1038/272528a0

Shennan, I., Long, A. J., Rutherford, M. M., Green, F. M., Innes, J. B., Lloyd, J. M., et al. (1996). Tidal marsh stratigraphy, sea-level change and large earthquakes, I: A 5000 year record in Washington, U.S.A. *Quaternary Science Reviews*, *15*(10), 1023–1059. https://doi.org/10.1016/S0277-3791(96)00007-8

Smith, S. M. (2009). Multi-decadal changes in salt marshes of Cape Cod, MA: Photographic analyses of vegetation loss, species shifts, and geomorphic change. *Northeastern Naturalist*, *16*(2), 183–208. https://doi.org/10.1656/045.016.0203

Snedden, G. A., Cretini, K., & Patton, B. (2015). Inundation and salinity impacts to above- and belowground productivity in *Spartina patens* and *Spartina alterniflora* in the Mississippi River deltaic plain: Implications for using river diversions as restoration tools. *Ecological Engineering*, *81*, 133–139. https://doi.org/10.1016/j.ecoleng.2015.04.035

Spencer, T., Schuerch, M., Nicholls, R. J., Hinkel, J., Lincke, D., Vafeidis, A. T., et al. (2016). Global coastal wetland change under sea-level rise and related stresses: The DIVA Wetland Change Model. *Global and Planetary Change*, *139*, 15–30. https://doi.org/10.1016/j.gloplacha.2015.12.018

Talke, S. A., Kemp, A. C., & Woodruff, J. (2018). Relative sea level, tides, and extreme water levels in Boston Harbor from 1825 to 2018. *Journal of Geophysical Research: Oceans*, *123*(6), 3895–3914. https://doi.org/10.1029/2017JC013645

Temmerman, S., Bouma, T. J., Govers, G., & Lauwaet, D. (2005). Flow paths of water and sediment in a tidal marsh: Relations with marsh developmental stage and tidal inundation height. *Estuaries*, *28*(3), 338–352. https://doi.org/10.1007/BF02693917

Temmerman, S., Govers, G., Wartel, S., & Meire, P. (2003). Spatial and temporal factors controlling short-term sedimentation in a salt and freshwater tidal marsh, Scheldt estuary, Belgium, SW Netherlands. *Earth Surface Processes and Landforms*, *28*(7), 739–755. https://doi.org/10.1002/esp.495

Tetra Tech EC, Inc. (2005). Comprehensive site assessment report: Fireworks I.

Turner, R. E., Howes, B. L., Teal, J. M., Milan, C. S., Swenson, E. M., & Tonerb, D. D. G. (2009). Salt marshes and eutrophication: An unsustainable outcome. *Limnology & Oceanography*, *54*(5), 1634–1642. https://doi.org/10.4319/lo.2009.54.5.1634

University of Massachusetts Amherst. (1952). *Department of Forestry and Wildlife Management. Plymouth County: Aerial Photograph, August 19, 1951. William P. MacConnell Aerial Photograph Collection (FS 190)*. Special Collections and University Archives, University of Massachusetts Amherst Libraries.

US Air Force. (1960). AF-59-33B R-79. Image 7891, Scituate, Massachusetts.

Van Dyke, E., & Wasson, K. (2005). Historical ecology of a central California estuary: 150 years of habitat change. *Estuaries*, *28*(2), 173–189. https://doi.org/10.1007/BF02732853

VanZomeren, C. M., Berkowitz, J. F., Piercy, C. D., & White, J. R. (2018). Restoring a degraded marsh using thin layer sediment placement: Short term effects on soil physical and biogeochemical properties. *Ecological Engineering*, *120*, 61–67. https://doi.org/10.1016/j.ecoleng.2018.05.012

Voss, C. M., Christian, R. R., & Morris, J. T. (2013). Marsh macrophyte responses to inundation anticipate impacts of sea-level rise and indicate ongoing drowning of North Carolina marshes. *Marine Biology*, *160*(1), 181–194. https://doi.org/10.1007/s00227-012-2076-5

Watson, E. B. (2004). Changing elevation, accretion, and tidal marsh plant assemblages in a South San Francisco Bay tidal marsh. *Estuaries*, *27*(4), 684–698. https://doi.org/10.1007/BF02907653

Watson, E. B., Wigand, C., Davey, E. W., Andrews, H. M., Bishop, J., & Raposa, K. B. (2017). Wetland loss patterns and inundation-productivity relationships prognosticate widespread salt marsh loss for southern New England. *Estuaries and Coasts*, *40*(3), 662–681. https://doi.org/10.1007/s12237-016-0069-1

Wheatcroft, R. A., & Sommerfield, C. K. (2005). River sediment flux and shelf sediment accumulation rates on the Pacific Northwest margin. *Continental Shelf Research*, *25*(3), 311–332. https://doi.org/10.1016/j.csr.2004.10.001

White, W. A., & Tremblay, T. A. (1995). Submergence of wetlands as a result of human-induced subsidence and faulting along the upper Texas Gulf Coast. *Journal of Coastal Research*, *11*, 788–807.

Wigand, C., Roman, C. T., Davey, E., Stolt, M., Johnson, R., Hanson, A., et al. (2014). Below the disappearing marshes of an urban estuary: Historic nitrogen trends and soil structure. *Ecological Applications*, *24*(4), 633–649. https://doi.org/10.1890/13-0594.1

Wolters, S., Zeiler, M., & Bungenstock, F. (2010). Early Holocene environmental history of sunken landscapes: Pollen, plant macrofossil and geochemical analyses from the Borkum Riffgrund, southern North Sea. *International Journal of Earth Sciences*, *99*(8), 1707–1719. https://doi.org/10.1007/s00531-009-0477-6

Woodruff, J. D., Venti, N. L., Mabee, S. B., DiTroia, A. L., & Beach, D. (2021). Grain size and beach face slope on paraglacial beaches of New England, USA. *Marine Geology*, *438*, 106527. https://doi.org/10.1016/j.margeo.2021.106527

Wright, A. J., Edwards, R. J., & van de Plassche, O. (2011). Reassessing transfer-function performance in sea-level reconstruction based on benthic salt-marsh foraminifera from the Atlantic coast of NE North America. *Marine Micropaleontology*, *81*(1–2), 43–62. https://doi.org/10.1016/j.marmicro.2011.07.003

Yellen, B., Woodruff, J., Ladlow, C., Ralston, D. K., Fernald, S., & Lau, W. (2021). Rapid tidal marsh development in anthropogenic backwaters. *Earth Surface Processes and Landforms*, *46*(3), 554–572. https://doi.org/10.1002/esp.5045

Yellen, B., Woodruff, J., Ralston, D., Ladlow, C., Fernald, S., & Lau, W. (2020). Rapid tidal marsh development in anthropogenic backwaters (preprint). *Earth*. https://doi.org/10.31223/osf.io/ga5pm

Yellen, B., Woodruff, J. D., Cook, T. L., & Newton, R. M. (2016). Historically unprecedented erosion from Tropical Storm Irene due to high antecedent precipitation. *Earth Surface Processes and Landforms*, *41*(5), 677–684. https://doi.org/10.1002/esp.3896